Aus der Medizinischen Klinik mit Schwerpunkt Hepatologie und
Gastroenterologie der Medizinischen Fakultät
Charité – Universitätsmedizin Berlin

DISSERTATION

Generation of colon assembloids modeling epithelial-stromal interaction and self-organization

Erzeugung von Kolon-Assembloiden zur Modellierung der Epithel-Stroma Interaktion und Selbstorganisation

zur Erlangung des akademischen Grades
Doctor medicinae (Dr. med.)

vorgelegt der Medizinischen Fakultät
Charité – Universitätsmedizin Berlin

von

Manqiang Lin
aus Fuzhou, China

Datum der Promotion: 03.03.2023

Table of contents

List of tables

List of figures

List of abbreviations

3D	Three-dimensional
ACTA2	Actin alpha 2
ALI	Air-liquid interface
Ang-1	Angiopoietin-1
AOM	Azoxymethane
BEST4	Bestrophin 4
BMP	Bone morphogenetic protein
Bmpr1a	BMP receptor type 1a
$Bmpr1a^{\triangle EPI}$	Epithelium-specific Bmpr1a KO
$Bmpr1a^{\triangle MES}$	Mesenchyme-specific Bmpr1a KO
BMPRII	BMP receptor type 2
BSA	Bovine serum albumin
cDNA	Complementary DNA
COL1A2	Collagen type I alpha 2 chain
COVID-19	Coronavirus disease-2019
CSF1	Colony-stimulating factor 1
DMEM	Dulbecco’s Modified Eagle’s Medium
DSS	Dextran sodium sulfate
DTT	Dithiothreitol
EDTA	Ethylenediaminetetraacetic acid
ENS	Enteric nervous system
FACS	Fluorescence-activated cell sorting
FBS	Fetal bovine serum
FGF	Fibroblast growth factor
FM	Full medium
FVS450	Fixable Viability Stain 450
Gapdh	Glyceraldehyde-3-phosphate dehydrogenase
GDF	Growth and differentiation factor
GDNF	Glial-derived neurotrophic factor
GREM1	Gremlin 1
H&E	Hematoxylin and eosin
HBSS	Hanks’ balanced salt solution

HULEC-5a	Human lung microvascular endothelial cell line-5a
IL	Interleukin
ISC	Intestinal stem cell
KO	Knock-out
KRT20	Keratin 20
LGR5	Leucine-rich repeat-containing G- protein coupled receptor 5
MAPK	Mitogen-activated protein kinase
mEGF	Mouse epidermal growth factor
Mgp	Matrix Gla protein
mNoggin	Mouse noggin
MUC2	Mucin 2
OP-1	Osteogenic protein-1
OTOP2	Otopetrin 2
PAMP	Pathogen related molecular pattern
PBS	Phosphate-buffered saline
PBST	Tween/PBS
PDGFRA	Platelet derived growth factor receptor alpha
Pen/Strep	Penicillin / streptomycin
PFA	Paraformaldehyde
PGE2	Prostaglandin E2
Porcn	Porcupine O-acyltransferase
Postn	Periostin
pSmad1/5/8	Phosphorylated Smad1/5/8
qRT-PCR	Quantitative reverse transcription PCR
Rspo	R-spondin
sm-ISH	single-molecule RNA *in situ* hybridization
sWnt	Surrogate Wnt
Syp	Synaptophysin
TA	Transit-amplifying
TGF	Transforming growth factor
Th cell	T helper cell
Tubb3	β3-tubulin
VEGF	Vascular endothelial growth factor
VIM	Vimentin

WCRN	sWnt, CHIR-99021, R-spondin 1, and noggin
WT	Wild-type
Yap	Yes-associated protein
α-SMA	α smooth muscle actin

Abstract

The colonic epithelium interacts closely with the surrounding mesenchymal stroma, consisting of diverse cell populations that have emerged as essential constituents of the stem cell niche. Understanding the effects of niche cell-derived factors that control epithelial behavior has been made possible by organoid technology, mimicking the stem cell niche through supplementation of several growth factors. However, organoid culture models lack stromal cells, which currently limits the progress in our understanding of the bidirectional interplay between epithelium and stroma.

In this study, I established a colon assembloid culture system that includes both primary murine epithelial and stromal cells to investigate the crosstalk between these two compartments in the context of crypt development and homeostasis. I found that assembloids form mature crypts with directional cellular turnover and differentiation, which mimics *in vivo* epithelial crypt organization. Importantly, several key signaling pathways such as Wnt are activated in assembloids without supplementation of growth factors, which are required for proliferation and stemness in pure epithelial culture, indicating that stromal cells are sufficient to induce epithelial stemness. Assembloids imitate not only the epithelial but also the stromal architecture of colonic crypts *in vivo* to a great extent, recapitulating the diversity and spatial distribution of stromal cells including recently discovered subtypes such as telocytes and trophocytes with specific functional properties. Telocytes and trophocytes in assembloids exhibit a polarized distribution of BMP signaling molecules along the crypt axis, which I found to be crucial for the formation of signaling gradients and cellular differentiation along the crypt axis. Moreover, I observed that epithelial cells that exit the stem cell niche initiate Bmp2 expression, which is further augmented via a positive feed-forward loop between the epithelium and the stroma to enforce cell differentiation. Differentiating epithelial cell-derived Bmp2 induces a functional transition of stromal cells from the trophocyte state into the telocyte state, which further stabilizes BMP signaling by expressing Bmp2 itself. Using genetically heterogeneous assembloids, I demonstrated that activation of BMP signaling in both the epithelium and the stroma is essential for proper epithelial cell specification and crypt formation.

Taken together, this study reveals a bidirectional cross-communication between the epithelium and its surrounding stroma: on the one hand, the stroma provides key growth

factors required for crypt formation, while, on the other hand, signals from the epithelium ensure functional compartmentalization of stromal cell subsets – which together represent important prerequisites for mucosal self-organization.

Zusammenfassung

Das Kolonepithel steht in enger Wechselwirkung mit dem mesenchymalen Stroma, das wiederum verschiedene Zelltypen umfasst, die wichtige Bestandteile der Stammzellnische sind. Das Verständnis von Nischfaktoren, die das epitheliale Verhalten kontrollieren, wurde durch die Organoidtechnologie, in der die Stammzellnische durch Hinzugabe von diversen Wachstumsfaktoren nachgeahmt wird, ermöglicht. Allerdings beinhalten Organoidkulturen keine Stromazellen, sodass aktuell unser weiteres Verständnis des bidirektionalen Zusammenspiels von Epithel und Stroma limitiert ist.

Zur Erforschung des Zusammenspiels dieser zwei Kompartimente im Kontext der Kryptentwicklung und Homöostase habe ich in dieser Arbeit ein Kolon Assembloid-Kultursystem etabliert, das primäre Mausepithel- und -stromazellen enthält. Ich fand heraus, dass Assembloide reife Krypten mit gerichtetem Zellumsatz und Differenzierung bilden, welche die Kryptenorganisation *in vivo* nachbilden. Zudem sind in Assembloiden diverse wesentliche Signalwege wie Wnt ohne Zugabe von Wachstumsfaktoren aktiviert, sodass Stromazellen allein ausreichen, um eine epitheliale Stammzellaktivität zu induzieren. Dabei ahmen Assembloide nicht nur die epitheliale, sondern auch die mesenchymale Kryptenarchitektur *in vivo* weitgehend nach und spiegeln auch die Vielfalt und Verteilung von kürzlich identifizierten Stromazellsubtypen wie Telozyten und Trophozyten mit ihren spezifischen Funktionen wider. Telozyten und Trophozyten weisen eine polarisierte Verteilung von BMP-Molekülen entlang der Kryptenachse auf, die für die Entwicklung von Signalgradienten und zellulärer Differenzierung entlang der Kryptenachse wichtig ist. Darüber hinaus stellte ich fest, dass Epithelzellen, die die Stammzellnische verlassen, eine Bmp2-Expression auslösen, welche durch eine positive Vorwärtsschleife weiter verstärkt wird, sodass die zelluläre Differenzierung zunimmt. Bmp2 aus differenzierten Epithelzellen induziert einen funktionellen Übergang der Stromazellen aus dem Trophozytenzustand in den Telozytenzustand, der das BMP-Signal durch die Expression von Bmp2 selbst weiter stabilisiert. Mit genetisch heterogenen Assembloiden konnte ich nachweisen, dass die Aktivierung des BMP-Signals im Epithel als auch im Stroma für die ordnungsgemäße Spezialisierung der Epithelzellen und die Bildung der Krypten unerlässlich ist.

Zusammenfassend zeigt diese Studie eine bidirektionale Kommunikation zwischen dem Epithel und dem umgebenden Stroma. Einerseits stellt das Stroma wichtige Wachstumsfaktoren bereit, die für die Kryptenbildung erforderlich sind, andererseits sorgen Signale aus dem Epithel für eine funktionale Kompartimentierung von Stromazellsubtypen – beides sind wichtige Voraussetzungen für die Selbstorganisation der Schleimhaut.

1 Introduction

1.1 Colon

1.1.1 Anatomy and function

The colon is a critical part of the digestive system. In mammals, the colon comprises four segments: ascending colon, transverse colon, descending colon, and sigmoid colon. Although the physiological structure of the colon can be divided into the above four segments, it is a continuous organic whole without strict structural boundaries. When looking into the colon tissue from the inside to the outside, the colon wall is divided into the mucosa, submucosa, muscularis, and serosa. The colonic mucosa forms a high semi-circular fold into the intestinal lumen. Since no villi are formed, the mucosal surface is relatively flat. The mucosa is divided into the epithelium, lamina propria, and muscular mucosae. The epithelium comprises crypts formed by monolayer columnar epithelial cells, and is surrounded by the stroma in the lamina propria, which contains abundant mesenchymal cells and capillary/lacteal networks. Beneath the lamina propria, the muscularis mucosa comprises the outer longitudinal and inner circular muscle layers. The surrounding muscularis mucosa, the submucosa, forms loose connective tissue containing numerous blood vessels, lymphatic vessels, nerves, and fat cells. Similar to but much thicker than the muscularis mucosa, the muscularis is also composed of two smooth muscle layers that are inner circular and outer longitudinal. The outermost layer, the serosa, is a thin layer of mesothelium covering the colon[1].

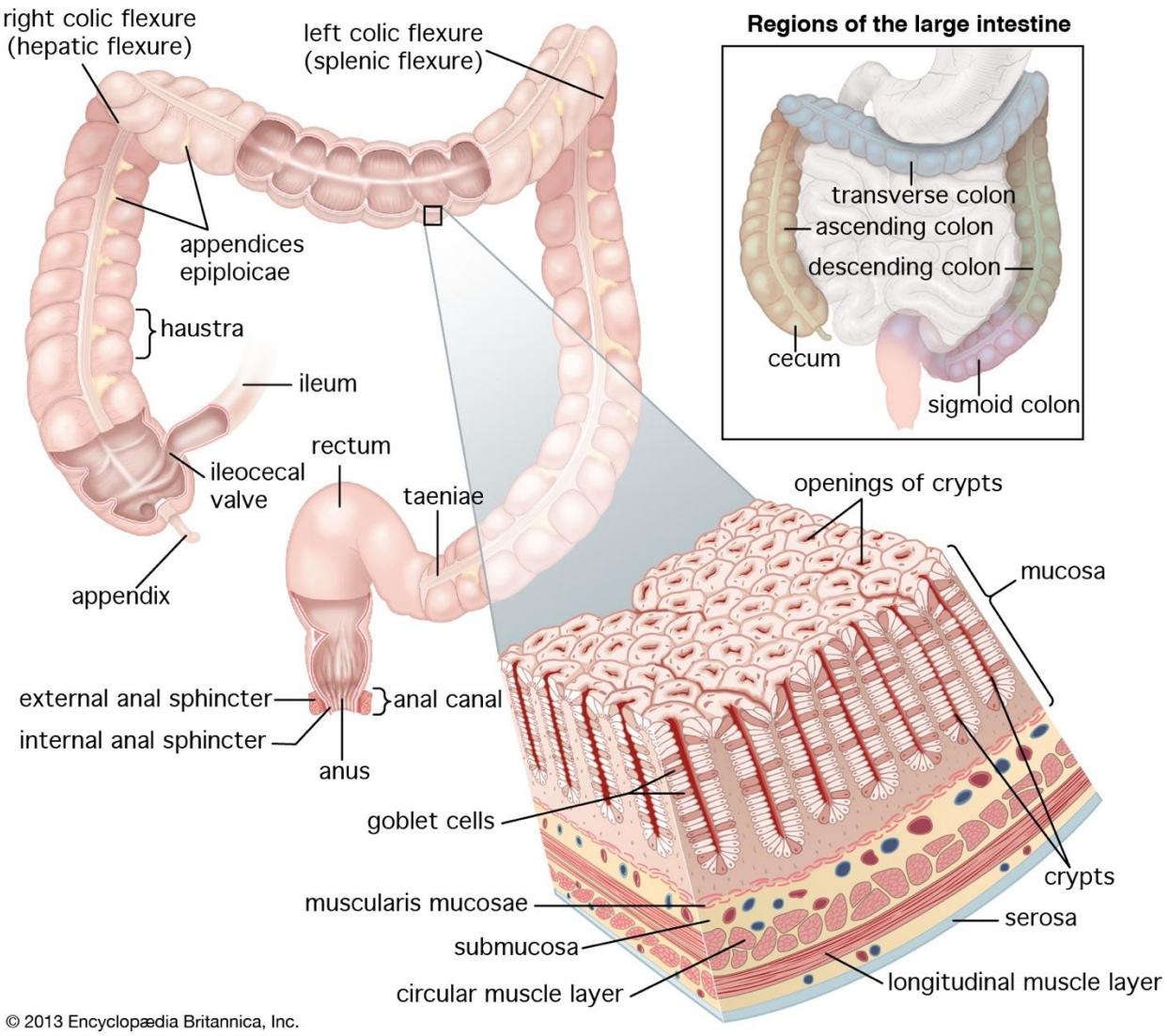

Figure 1 Structures of the human large intestine.

The human colon comprises four segments: ascending colon, transverse colon, descending colon, and sigmoid colon. The colon wall is divided into mucosa, submucosa, muscularis (circular and longitudinal muscle layers), and serosa. Image adopted from Encyclopaedia Britannica (https://www.britannica.com/science/large-intestine#/media/1/330544/68639).

The colon is mainly responsible for absorbing nutrients from digestive residues, maintaining the electrolyte balance, storing feces, and creating a habitat for microbiota. The absorption function of the colon is strong in the right half of the colon, absorbing mainly water and sodium, as well as small amounts of potassium, chlorine, urea, glucose, and amino acids. The colonic mucosa secretes mucus to form the first defense line and lubri-

cates stool for excretion. The colon has no digestive function. However, the resident microbiota has digestive effects and produces essential substances such as vitamins for the host[1].

1.1.2 Colonic epithelium

The colonic epithelium is composed of a monolayer and is organized into clonal crypts representing sophisticated anatomical and functional tissue units. The epithelial stem cells at each colonic crypt base, which are marked by Leucine-rich repeat-containing G-protein coupled receptor 5 (LGR5)[2], constantly divide and self-renew, giving rise to transit-amplifying (TA) cells that rapidly proliferate in the lower part of crypts[1,3]. TA cells subsequently differentiate into short-lived differentiated lineages, such as absorptive enterocytes, secretory goblet cells, and enteroendocrine cells[1,3,4].

The enterocytes marked by keratin 20 (KRT20) are highly polarized cells with microvilli and are located mainly at the crypt top[3]. The brush-like border at the surface of enterocytes increases the area of absorption and facilitates dietary nutrient uptake[3]. Only 14% of the cells from the colon are enterocytes, whereas enterocytes are highly enriched in the ileum[5]. In contrast, the colon has three times more goblet cells compared to the ileum (20% vs. 5%)[5]. Goblet cells mainly secrete mucin 2 (MUC2) which forms a thick viscous network with water, inorganic salts and antimicrobial peptides, namely the intestinal mucus barrier[6,7]. The mucus layers play a dual role of lubrication and physical barrier between intestinal contents and intestinal epithelium[6]. It is the first line of defense of the gastrointestinal tract against exogenous irritants and pathogenic bacteria[8]. In addition to goblet cells, enteroendocrine cells are another cell type that belong to the secretory lineage, representing 1% of epithelial cells in the intestine[9]. Enteroendocrine cells are critical sensors of metabolites of the intestinal flora[10]. They can recognize pathogen-associated molecular patterns (PAMPs) and produce essential cytokines, which directly orchestrates mucosal immunity[10]. Recently, some new epithelial cell subsets have been discovered, such as tuft cells and bestrophin 4 (BEST4) / otopetrin 2 (OTOP2) cells, which also play a significant role in intestinal homeostasis[4,11].

1.1.3 Colonic mesenchyme

The colonic mesenchymal stroma, which is closely associated with the epithelium, consists of a network of mesenchymal cell types comprising fibroblasts, myofibroblasts, endothelial cells, pericytes, immune cells, neurons, and glial cells[12]. These diverse cell types have emerged as essential constituents of the stem cell niche which contributes to epithelial stem cell homeostasis[12-17].

The enteric nervous system (ENS), composed of neurons and glial cells, drives coordinated bowel movements by controlling the muscular layer to ensure proper mixing and motion of gut contents[16]. Enteric neurons have close interactions between epithelial, stromal, and immune cells. Moreover, ENS was shown to express numerous risk genes related to neuropathic, inflammatory, and extra-intestinal diseases, suggesting a significant role in the occurrence of diseases[16]. Indeed, ENS dysfunction could cause several neurologic disorders, such as Hirschsprung's disease, autism spectrum disorders, and Parkinson's disease[16]. During intestinal epithelial recovery after injury, the enteric glial cells release diverse niche factors such as glial-derived neurotrophic factor (GDNF), epidermal growth factor (EGF), and transforming growth factor (TGF)-β1 to regulate tissue repair[16].

Immune cells respond to pathogenic infection and safeguard intestinal homeostasis by collaborating with epithelial cells, which are the body's first line of defense against pathogens[18]. Stimulated by pathogenetic factors, immune cells produce chemokines and cytokines to manipulate inflammation[18]. Extensive evidence shows that immune cells also modulate intestinal stem cell renewal and differentiation[19,20]. Co-cultures of small intestine organoids with Treg cells or innate lymphoid cells or stimulation of interleukin (IL)-10 or IL-22 promote intestinal stem cell (ISC) renewal[17]. Conversely, co-cultures with T helper (Th)1, Th2, or Th17 cells or treatment with IL-13 or IL-17 all impair ISC pool[17]. In addition, colony-stimulating factor 1 (CSF1) secreted by macrophages could also support ISC maintenance[21], while specific porcupine O-acyltransferase (Porcn) deletion in macrophages hinder epithelial repair after radiation damage[22].

Endothelial cells that form the inner lining of vessels are not passive conduits for delivering blood and lymph[15]. The endothelium pervades the ISC niche through capillaries and

lacteals and supply angiocrine factors, including growth factors, morphogens, extracellular matrix components and chemokines to modulate stem cell renewal, organ metabolism, and regeneration[15]. For instance, R-spondin (RSPO) produced by endothelial cells prevents intestinal epithelial damage and supports survival of ISC[23].

Pericytes surround the surface of the vessels and interact with the underlying endothelial cells to support the vascular structure and endothelial homeostasis[24,25]. It has been shown that pericytes play a critical role in angiogenesis and maturation of the newly formed vessels by producing vascular endothelial growth factor (VEGF)[26], angiopoietin-1 (Ang-1)[27], and TGF-β[25].

Myofibroblasts share similar features with smooth muscle cells and fibroblasts, which express both contractile markers like alpha-smooth muscle actin (α-SMA, encoded by *actin alpha 2* [*ACTA2*]) and pan-fibroblast marker genes, such as vimentin (*VIM*) and collagen type I alpha 2 chain (*COL1A2*)[12]. In the gastrointestinal tract, myofibroblasts that reside in the muscularis mucosa secrete Wnt and R-spondin3 to regulate stem cell homeostasis during infection and injury[13,28].

Fibroblasts are an abundant and heterogeneous stromal population that expresses platelet-derived growth factor receptor alpha (PDGFRA), COL1A2, and VIM[12]. Several subsets of stromal fibroblasts, such as trophocytes and telocytes, have been characterized as a critical source of growth factors (Wnt ligands, R-spondins, gremlin 1 [GREM1]) and morphogens (bone morphogenetic proteins [BMPs] and Wnt5a) that generate gradients of signaling, and promote epithelial stem cell self-renewal, proliferation, and directed cellular differentiation[12,29,30]. Other distinct fibroblast sub-populations have also been shown to promote regeneration by augmenting Wnt signaling[31], induce factors that impair epithelial turnover and exacerbate disease severity during colitis[12], or produce prostaglandin E2 (PGE2) to activate yes-associated protein (YAP) in intestinal epithelium and thus drive tumor initiation[32].

1.2 Organoid culture system

The organoid is a three-dimensional primary cell culture technology that allows mammalian stem cells to show their self-organizing capacity, and therefore resemble crucial structures and functions of organs such as the gut[33]. Gastrointestinal organoids can be derived from two types of stem cells: pluripotent stem cells and adult stem cells[34]. Applying growth factor cocktails in a stepwise manner, pluripotent stem cells are capable of differentiating into cell types of diverse organs[34]. Distinct from pluripotent stem cells, adult stem cells that are obtained from specific adult organs were previously believed to be incapable of proliferating *in vitro* in the long term[34]. However, a series of studies have developed a culture condition comprised of basement membrane extract and key stem cell niche factors that maintains stable stem cell renewal[34]. A small intestine organoid culture can be established with single $Lgr5^+$ stem cells or whole crypts suspended in a laminin-rich extracellular matrix (e.g. Matrigel) and cultured in serum-free medium supplemented with R-spondin1 or R-spondin3 (Wnt agonists), EGF, and the BMP inhibitor noggin[35]. For a colon organoid culture, additional Wnt activators such as surrogate Wnt (sWnt) or Wnt3a and CHIR-99021 are necessary due to the lack of Wnt-producing cells in the colonic epithelium[36,37].

Traditional cell lines that are immortalized may be genetically abnormal and do not represent all the cell types, cellular processes, and functions of *in vivo* organs. Primary organoid technology overcomes these shortcomings and appears to be a feasible and robust tool to explore cell biology. For instance, studying mechanisms underlying epithelial behaviors, such as proliferation and differentiation, have been made possible by manipulating growth factors in organoid culture medium[38]. Modeling infectious diseases is also among the key applications of organoid technology. During the recent coronavirus disease-2019 (COVID-19) pandemic, organoids were applied to investigate virus transmission in specific organs[39]. Organoids could be used to model hereditary diseases and cancers by generating mutant organoids or by culturing cells directly derived from patients' biopsy specimens[40]. Organoids derived from patients' cells allow a rapid assessment of drug response and identification of the optimal treatment for the individual patient[40]. Furthermore, organoid technology is a promising tool of regenerative medicine. Several studies have shown a successful transplantation of organoids into animals after *in vitro* stem cell expansion[41].

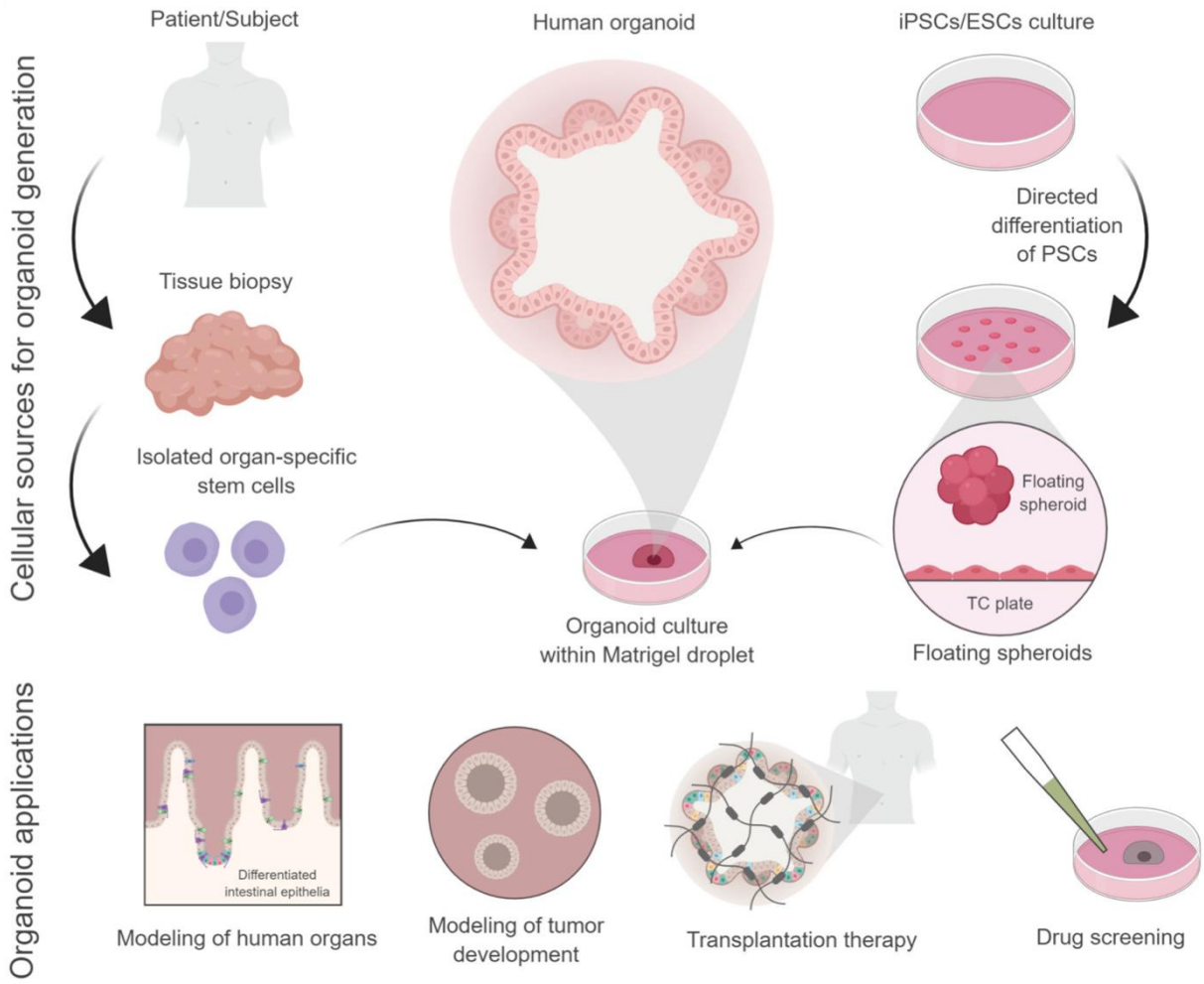

Figure 2 The organoid technology and applications.

e Image adopted from Cruz-Acuña R and García AJ[42].

1.3 BMP signaling

BMPs are members of the TGF-β superfamily, and include BMP 2/4/5/6/7/8/9/10, growth and differentiation factor (GDF) 5–7, and osteogenic protein-1 (OP-1)[43]. When extracellular BMPs bind to BMP receptor type 2 (BMPRII), BMPRII phosphorylates and activates BMPRI, which in turn recruits and phosphorylates Smad proteins Smad1/5/8 that are intracellular signal transducers of BMP signaling[43]. Phosphorylated Smad1/5/8 (pSmad1/5/8) forms a complex with Smad4 and then translocates to the nucleus to regulate target gene transcription[43]. In addition to canonical BMP signaling mediated by

Smad, BMP receptors can also transduce signals via Smad-independent pathways (non-canonical BMP signaling), including activation of the mitogen-activated protein kinase (MAPK) pathway[44]. BMP signaling activities can be modulated by their antagonists (e.g. Grem1, noggin) in the extracellular compartment[45]. BMP antagonists associate with BMP ligands and thus avoid binding between ligands and receptors[45].

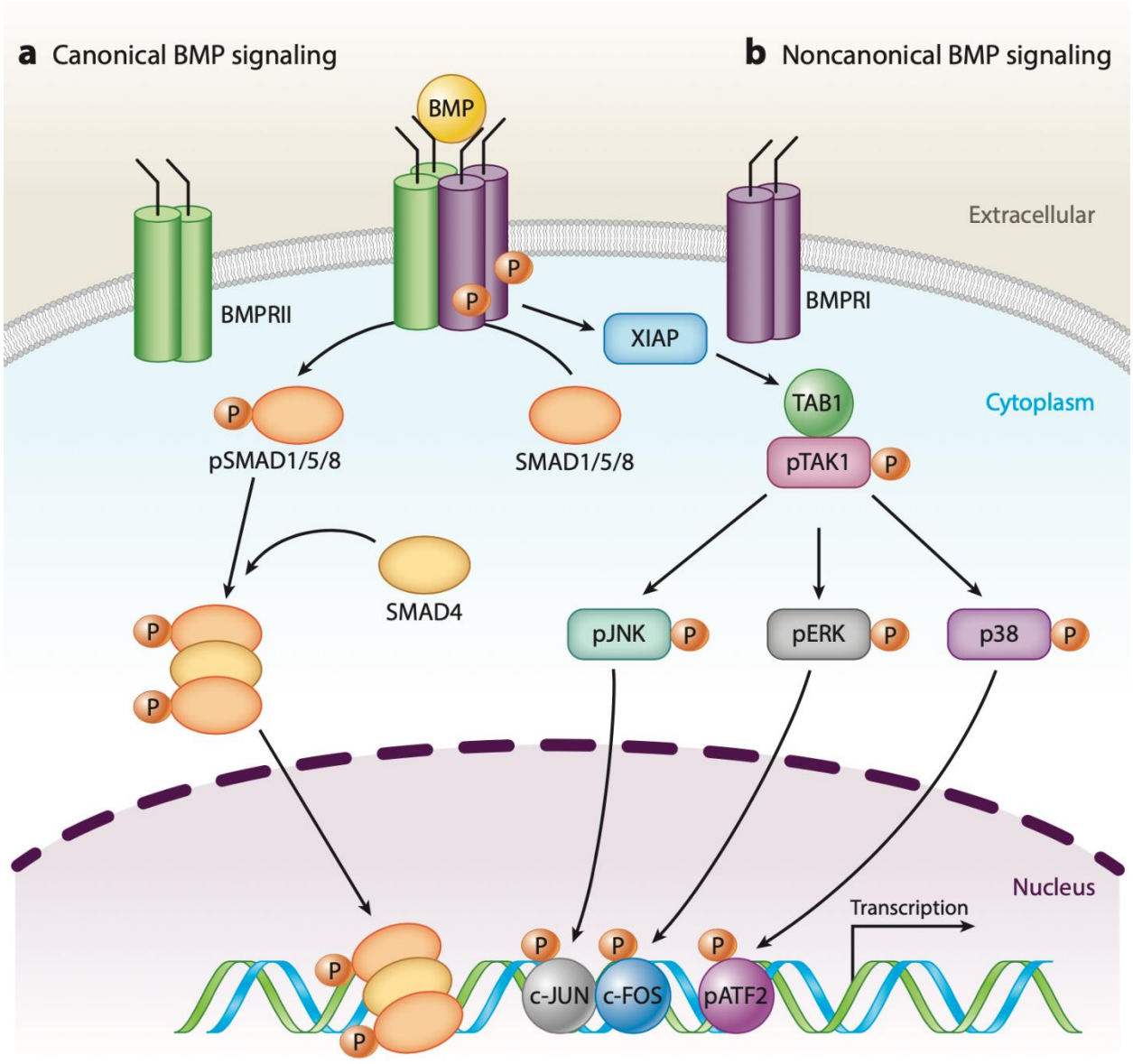

Figure 3 BMP signaling pathway.

Canonical BMP signaling (**a**) is mediated by Smad proteins, while noncanonical BMP signaling (**b**) can be transduced by activating mitogen-activated protein kinases (MAPKs), such as JNK, ERK, and p38. Image adopted from Zhang Y and Que J[43].

BMP ligands and receptors are extensively expressed in the gastrointestinal tract[43]. Of note, BMP2 and BMPRIA are located in both the epithelium and the mesenchyme of the lamina propria, indicating bidirectional cross-talk between these two compartments[29,46-48]. Through epithelial-mesenchymal interactions, BMP signaling plays a critical role in embryo development, cell turnover, inflammation, and tumorigenesis[43]. During early patterning of the gut, BMP signaling coordinates with other pathways (e.g. Wnt, NOTCH, FGF, and Hedgehog) and specifies the primitive gut tube into the foregut, midgut, and hindgut[49-54]. Furthermore, BMP drives the maturation of mucosa lining the foregut-, midgut-, and hindgut-derived gastrointestinal tract[55]. In the intestine, BMP signaling is one of the central players to regulate epithelial cell differentiation[56]. BMP directly inhibits ISC signature gene expression[48], but drives terminal differentiation of goblet cells and Paneth cells[57]. A deficiency of BMP signaling either in the epithelium or the mesenchyme causes epithelial/stromal hyperproliferation, impairs cell differentiation, promotes inflammation, and eventually leads to polyposis initiation[47,48,58-60]. Notably, BMP signaling has opposite effects at different tumor stages. Previous studies showed that BMP suppresses cancer formation but promotes cancer invasion and metastasis at advanced stages, which might be dependent on the status of Smad4 and p53[61,62].

1.4 Objective of this study

Colonic epithelial stem cells at each crypt base constantly divide and self-renew, giving rise to short-lived differentiated lineages[3]. The epithelium interacts closely with various stromal cells. Several subsets of stromal cells, such as trophocytes and telocytes, have been recognized as a crucial source of growth factors and morphogens that modulate epithelial cell turnover[14,29]. Although the organoid model has become an essential tool to study the gastrointestinal epithelium, the current organoid systems usually consist only of epithelial cells, and there is a dearth of powerful tools to explore the interdependency between the epithelium and the stroma, which currently limits progress in our understanding of the gastrointestinal mucosa as a whole. The objective of this study was to establish a primary colonic cell co-culture system to model *in vivo* epithelial-stromal crosstalk and self-organization. Initially, I generated the colon assembloid culture system that integrates various cell types to determine whether this system enables the generation of true colonic

crypts that resemble the *in vivo* anatomy, cellular organization, signaling gradients, and directional epithelial turnover. Next, I used the assembloid model to study the impact of epithelial-stromal interaction on colonic crypt formation and stromal cell functions via BMP signaling. Additionally, the aim was to explore morphological and biological characteristics of colon tumor assembloids.

2 Materials and methods

2.1 Materials

2.1.1 Mice

Table 1 Mouse strains used in the study.

Name	Description	Reference
C57BL/6	Standard wild-type mice	Charles River Laboratory
Axin2CreErt2/ Rosa26-tdTomato	Cre recombinase expression under *Axin2* promotor, which upon activation by tamoxifen induces conditional *Rosa26-tdTomato* lineage tracing. These mice were generated by breeding *Axin2CreErt2* to *Rosa26-tdTomato* mice.	van Amerongen R, et al. Cell Stem Cell. 2012; 11(3):387-400.[63] Madisen L, et al. Nat Neurosci. 2010;13(1):133-40.[64]
Axin2CreErt2/ Bmpr1a$^{fl/fl}$	Cre recombinase expression under Axin2 promotor, which upon activation by tamoxifen induces conditional Bmpr1a knockout. Mice were generated by breeding Axin2CreErt2 to Bmpr1a$^{fl/fl}$ mice.	van Amerongen R, et al. Cell Stem Cell. 2012; 11(3):387-400.[63] Mishina Y, et al. Genesis. 2002;32(2):69-72.[65]
Bmpr1a$^{fl/fl}$	These floxed mutant mice possess three loxP sites flanking *Bmpr* locus (intron 1 and intron 2) and removal of the flanked regions results in loss of expression of Bmpr1a.	Mishina Y, et al. Genesis. 2002;32(2):69-72.[65]
tg Act-CFP	These mice express cyan fluorescent protein under the control of the chicken beta-actin promoter.	Hadjantonakis AK, et al. BMC Biotechnol. 2002; 2(1):11.[66]
tg Act-DsRed	These mice express the red fluorescent protein variant DsRed.MST under the control of the chicken beta-actin promoter.	Vintersten K, et al. Genesis. 2004;40(4):241-6.[67]

2.1.2 Cell culture reagents

Table 2 Commercially available primary cell culture reagents and supplements.

Name	Supplier

4OH-tamoxifen	Sigma
A83-01	Sigma
Advanced Dulbecco's Modified Eagle's Medium (DMEM)/F12	Gibco
B27 supplement (50x)	Gibco
CHIR-99021	Selleckchem
Cryo-SFM	PromoCell
Cultrex	R&D systems
Fetal bovine serum (FBS)	Gibco
GlutaMAX (100x)	Gibco
HEPES	Gibco
Matrigel, growth factor reduced, phenol red-free	Corning
Mouse epidermal growth factor (mEGF)	Invitrogen
Mouse noggin (mNoggin)	PeproTech
N-acetylcysteine	Sigma
N2 supplement (100x)	Gibco
Organoid harvesting solution	R&D systems
Penicillin / streptomycin (Pen/Strep)	Gibco
Surrogate Wnt (sWnt)	U-Protein Express
TAT-CRE Recombinase	Millipore
TryplE	Gibco
Y-27632 (ROCK inhibitor)	Hoelzel

Table 3 Primary cell culture supplements and media produced in-house.

Name	Preparation	Cell line
R-spondin1 conditioned medium	DMEM + 10 % FBS; selection by zeocin treatment (300 µg/ml; Invitrogen; #250-01) for 5 days. Conditioned media was collected after 5 and 10 days, centrifuged (300x g, 15 min) and sterile filtrated (0.22 µm filter).	293T HA-RSPO1-FC kindly provided by Prof. Hans Clevers, Hubrecht Institute, Utrecht, Netherlands

Table 4 Recombinant proteins.

Name	Supplier
BMP2	R&D systems
GREM1	R&D systems

2.1.3 Buffers and solutions

Table 5 General buffers and solutions.

Name	Preparation	Supplier
1x Phosphate-buffered saline (PBS)	-	Gibco
2% Ammonia water	ddH_2O, 2% ammonium hydroxide solution	-
4% paraformaldehyde	37-40g paraformaldehyde, 600ml ddH2O at 60-70°C, clear solution with NaOH, 100ml 10x PBS and ddH_2O to 1L; pH 7.4	-
Blocking buffer (Whole-mount staining)	3% BSA, 1% Saponin, 2% Triton X-100, 0.02% Na Azide	-
Blocking buffer (Immunofluorescence)	PBS, 1% BSA, 2% FBS, 0.1% Tween20	-
Calcium and magnesium-free Hanks' balanced salt solution (HBSS)	-	Gibco
DNase/RNase free water	-	Gibco
FACS buffer	PBS, 1% FBS, 1% HEPES, 0,5% DNase I, 3 µl/ml Y-27632	-
PBST	PBS, 0.1% Tween 20	-
RNAscope H_20_2 & Protease Plus Reagents	-	Advanced Cell Diagnostics
RNAscope Target Retrieval Reagents	-	Advanced Cell Diagnostics
RNAscope Wash Buffer Reagents	-	Advanced Cell Diagnostics

Target retrieval solution (10x Citrate buffer, pH 6.0)	ddH_2O, 100mM (29.4 g/L) sodium citrate dehydrate, citric acid (for pH adjustment)	-

2.1.4 Chemicals and consumables

Table 6 General chemicals and consumables.

Name	Supplier
Agarose	Sigma
Ammonium hydroxide	Sigma
Azoxymethane (AOM)	Sigma
Bovine serum albumin (BSA), Fraction V	Life Technologies
Cell strainer	Falcon
Citric acid	Sigma
Cover glasses	Marienfeld
CoverWell imaging chambers (whole-mount staining)	Grace Bio-labs
Dextran sodium sulfate (DSS)	MP Biomedical
Dithiothreitol (DTT)	Sigma
DNase I	Invitrogen
EcoMount (single-molecule RNA *in situ* hybridization)	Biocare Medical
Ethylenediaminetetraacetic acid (EDTA)	Invitrogen
Embedding Cassettes	Simport
Eosin	Roth
Ethanol	Merck
ImmEdge pen (single-molecule RNA *in situ* hybridization)	Vector
Immu-Mount (immunostaining)	Epredia
Liberase TL	Roche
Mayer's hematoxylin solution	Roth
Pap pen (immunostaining)	Kisker
Paraffin	Roth
Paraformaldehyde (PFA)	Sigma
Roti-Histokitt	Roth
Saponin	Riedel-de Haën

Sodium citrate dihydrate	Sigma
SuperFrost Plus gold adhesion microscope slides	Epredia
SuperFrost Plus microscope slides	R.Langenbrinck
SYBR green master mix	Thermo Fisher
Triton X-100	Calbiochem
Tween 20	Merck
UltraComp eBeads	Invitrogen
VectaMount Aqueous Mounting Medium (whole-mount staining)	Vector
Xylene	Roth

2.1.5 Commercial kits

Table 7 Commercial kits and their application.

Name	Application	Supplier
Chromium Single Cell Kits	Single-cell RNA sequencing	10X GENOMICS
iScript cDNA synthesis kit	cDNA synthesis	Bio-Rad
NucleoSpin RNA isolation kit	RNA isolation	Macherey & Nagel
RNAscope 2.5 HD Reagent Kit-RED	Single-molecule RNA *in situ* hybridization	Advanced Cell Diagnostics

2.1.6 Antibodies

Table 8 Primary antibodies for histological analysis.

Name	Dilution	Supplier	Catalog number
Alexa Fluor 647 fluorophore-conjugated phalloidin	1:100	Life Technologies	A22287
Goat anti-αSMA	1:100	Abcam	ab5694
Mouse anti-E-cadherin	1:200	BD	610181
Rabbit anti- active Yap1	1:200	Abcam	ab205270
Rabbit anti-Cd31	1:100	Cell Signaling Technology	77699T
Rabbit anti-Ki67	1:100	Cell Signaling Technology	9192

Rabbit anti-Krt20	1:100	Cell Signaling Technology	13063
Rabbit anti-Muc2 C3	1:1000	A gift from Prof. Gunnar C. Hansson	-
Rabbit anti-synaptophysin	1:50	Abcam	ab178412
Rabbit anti-vimentin	1:100	Cell Signaling Technology	5741S
Rabbit anti-β3-tubulin (Tubb3)	1:100	Cell Signaling Technology	5568T

Table 9 Secondary antibodies and other dyes for histological analysis.

Name	Dilution	Supplier	Catalog number
DAPI	1:300	Roche	10236276001
Donkey anti goat Alexa-Fluor 647	1:250	Jackson Immunoresearch	705-605-003
Donkey anti mouse Alexa-Fluor 488	1:250	Jackson Immunoresearch	715-546-150
Donkey anti rabbit Cy3	1:250	Jackson Immunoresearch	711-165-152

Table 10 Antibodies and dyes for flow cytometric analysis.

Name	Dilution	Supplier	Catalog number
Cd31 APC	1:200	BD	551262
Cd326 (EpCAM) PE	1:200	Miltenyi Biotec	130-117-779
Cd34 FITC	1:100	BD	560238
Cd45 APC-Cy7	1:200	BD	557659
FVS450	1:1000	BD	562247

2.1.7 RNA probes for single-molecule in situ hybridization (sm-ISH)

Table 11 RNA probes for sm-ISH.

Gene name	Target region	Supplier	Catalog number
Bmp2	854 - 2060	Advanced Cell Diagnostics	406661
Foxl1	954 - 1931	Advanced Cell Diagnostics	407401
Grem1	398 - 1359	Advanced Cell Diagnostics	314741
Rspo3	731-2164	Advanced Cell Diagnostics	402011

2.1.8 Primers for quantitative reverse transcription PCR (qRT-PCR)

Murine primers were designed with the BLAST online tool. Primers were diluted to 10µM before use. The melting temperature was determined to be 60 °C.

Table 12 Primers for quantitative reverse transcription PCR (qRT-PCR).

Gene name	Primer Sequence	Supplier
Bmp2	Forward 5'- GACTGCGGTCTCCTAAAGGTCG-3' Reverse 5'-CTGGGGAAGCAGCAACACTA-3'	Sigma
Cd34	Forward 5'-GGCCAATAGCACAGAACTTCC-3' Reverse 5'-CCCAACAGCCATCAAGGTTC-3'	Sigma
Foxl1	Forward 5'-TCATCATGGATCGCTTCCCG-3' Reverse 5'-CCTCTTCCTGCGCCGATAAT-3'	Sigma
Gapdh	Forward 5'- TCACCATCTTCCAGGAGCG-3' Reverse 5'-AAGCAGTTGGTGGTGCAGG-3'	Sigma
Grem1	forward 5'-AAGTGACAGAATGAATCGCACC-3' reverse 5'-CCTCAGCTGTTGGCAGTAGG-3'	Sigma
Id1	Forward 5'-GCTCTACGACATGAACGGCT-3' Reverse 5'-AACACATGCCGCCTCGG-3'	Sigma
Krt20	Forward 5'-GTCCCACCTCAGCATGAAAGA-3' Reverse 5'-TCTGGCGTTCTGTGTCACTC-3'	Sigma
Lgr5	Forward 5'-CCTACTCGAAGACTTACCCAGT-3' Reverse 5'-GCATTGGGGTGAATGATAGCA-3'	Sigma
Mgp	Forward 5'-CCGAGACACCATGAAGAGCC-3' Reverse 5'-GTTGCGTTCCTGGACTCTCTT-3'	Sigma
Rspo3	Forward 5'-TTGACAGTTGCCCAGAAGGG-3' Reverse 5'-CTGGCCTCACAGTGTACAATACT-3'	Sigma
Wnt5a	Forward 5'-ACGCTATACCAACTCCTCTGC-3' Reverse 5'-AATATTCCAATGGGCTTCTTCATGG-3'	Sigma

2.1.9 Laboratory instruments

Table 13 Laboratory instruments.

Machine	Application	Supplier
BD FACS Aria III flow cytometer	Fluorescence-activated single-cell sorting (FACS)	BD Bioscience
Cytek Aurora 3 laser spectral cytometer	Flow cytometry	CyTek Biosciences
Eppendorf centrifuge 5417C	Eppendorf tubes centrifugation	Eppendorf
Eppendorf centrifuge 5810R	Primary cell culture centrifugation	Eppendorf
EVOS M5000 imaging system	Live cell imaging	Invitrogen
Hera cell 150 Incubator	Primary cell culture	Heraeus
HistoCore AUTOCUT microtome	Tissue processing	Leica
HybEZ Oven	Single-molecule *in situ* hybridization	Advanced Cell Diagnostics
Logos One automat	Tissue paraffin embedding	Milestone
Mini Orbital Shaker for CO_2 Incubator	Cell culture	Edmund Buehler
NanoDrop One Microvolume UV/Visible Spectrophotometer	Measurments of RNA concentration	Thermo Fisher
Observer 7 microscope	imaging	Zeiss
PeqSTAR thermocycler	cDNA sythesis	Peqlab
QuantStudio 3 Real-Time PCR System	qRT-PCR	Thermo Fisher
TCS SP-8 microscope	Confocal microscopy	Leica

2.1.10 Software

Table 14 Software.

Name	Application	Supplier
Adobe Illustrator 2019 23.0.6	Figure processing	Adobe
EndNote 20	Citation formatting	Clarivate Analytics
FCS Express 7	Flow cytometry	De Novo
ImageJ 2.0.0 (Fiji)	Image processing and analysis	NIH

Imaris 9.8	Image processing	Oxford Instruments
Leica Application Suite X (LAS X)	Confocal imaging	Leica
Microsoft office 2019 16.57	Data collection, processing, and presentation	Microsoft
Prism 8	Data analysis and statistic	GraphPad
QuantStudio 3 Real-Time PCR Software v1.7.1	qRT-PCR	Thermo Fisher
RStudio1.4.1717	scRNA-seq data analysis	RStudio
Seurat v3 R package	scRNA-seq data analysis	Paul Hoffman, Satija Lab and Collaborators
ZEN 3.4	Imaging	Zeiss

2.2 Methods

2.2.1 Primary murine colon organoid culture

The murine colon was dissected, opened longitudinally, and cut into 1-cm pieces. The tissue was washed three times in 1X phosphate-buffered saline (PBS), followed by incubation for 20 min in 10 mM EDTA/PBS supplemented with 0.5 mM Dithiothreitol (DTT) at 37 °C. The buffer was changed to ice-cold PBS, and the tube was vigorously shaken for 30 sec to isolate colonic crypts. The supernatant containing crypts was collected and centrifuged at 400 g for 5 min at 4 °C, and tissue fragments were used for stromal cell isolation. The number of colonic crypts was determined, and 150 crypts were resuspended and seeded in a 10-µl drop of Matrigel (or Cultrex) in a 24-well plate (three drops per well). Matrigel was polymerized at 37 °C for 15 min and then 500 µl medium were added for each well: Advanced Dulbecco's Modified Eagle's Medium (DMEM)/F12 containing 10 mM HEPES, 2 mM GlutaMAX, 100 U/mL penicillin/streptomycin, 1.25 mM N-acetylcysteine, 1X B-27, 1X N2, 50 ng/mL mouse epidermal growth factor (EGF), and 0.5 µM A38-01, which was supplemented with 0.328 nM surrogate Wnt (sWnt), 3 µM CHIR-99021, 25 % R-spondin 1 conditioned medium, and 100 ng/mL mouse noggin for maintenance in the full medium (FM) condition (Table 15). 10 µM Y-27632 (Rock inhibi-

tor) were added after the initial seeding and after passaging. The organoids were incubated at 37 °C in a humidified incubator with 5 % CO_2. The medium was replaced every 1-2 days. Every 4-5 days, the organoids were passaged as single cells after a 5-minute incubation in TryplE at 37 °C. A total of 2500 cells were seeded per 10 µl Matrigel drop in a 24-well plate (three drops per well). The organoids were cultured for at least one passage before specific experiments were carried out. To freeze organoids, single cells were suspended in 500 µl Cryo-SFM freezing medium and the organoid cells were transferred to a cryovial. The vial was placed in an isopropanol-containing freezing container and kept overnight at -80 °C.

Table 15 Composition of colon organoid medium.

Reagent	Volume (per 1 ml medium)	Final concentration
A83-01	1 µL	0.5 µM
Advanced DMEM/F-12	679.5 µL	-
B27 supplement (50x)	20 µL	1x
CHIR-99021*	1 µL	3 µM
Glutamax	10 µL	2 mM
HEPES	10 µL	10 mM
mouse epidermal growth factor (EGF) *	1 µL	50 ng/mL
mouse noggin	1 µL	100 ng/mL
N-acetylcysteine	2.5 µL	1.25 mM
N2 supplement (100x)	10 µL	1x
Penicillin/Streptomycin	10 µL	100 U/ml
R-spondin-1 conditioned medium	250 µL	25%
surrogate Wnt (sWnt) *	2 µL	0.328 nM
Y-27632	3 µL	10 µM

* sWnt was prediluted to 1:100; mEGF and CHIR-99021 were prediluted to 1:10.

Where indicated, sWnt, CHIR-99021, R-spondin 1, and noggin were withdrawn (-WCRN) for 48 hours to induce organoid differentiation after two days of culture in FM. For BMP2 treatment, organoids were cultured in FM for two days followed by 48 hours of culture

with specified concentrations of recombinant mouse BMP2 (rBMP2) and removal of noggin. To generate *Bmpr1a* knock-out (KO) organoids, 1.5 µM 4OH-tamoxifen were added to organoids derived from *Axin2CreErt2/Bmpr1a*$^{fl/fl}$ mice for 24 hours.

2.2.2 Primary murine colon stromal cell culture

To isolate colon stromal cells, the tissue fragments were further processed from crypt isolation. The tissue fragments were washed four times with ice-cold PBS and shaken after every wash to remove epithelium. When clean supernatant was obtained, the tissue fragments were cut into tiny pieces and incubated in calcium and magnesium-free HBSS containing Liberase TL (1 unit/mL) and DNase I (1 unit/mL) at 37 °C for 1 hour, with pipetting every 10 min. Every 20 min, the digested fraction was collected and put into an ice-cold stromal cell medium containing Advanced DMEM/F12, 10 % fetal bovine serum (FBS), 100 U/mL penicillin/streptomycin, and 10 µM Y-27632 (Table 16). The collected fraction was filtered through a 70-µm cell strainer and centrifuged at 400 g for 5 min at 4 °C. Colon stromal cells were seeded on 12- or 6-well plates, or 75 cm^2 flasks, and cultured in a stromal cell medium.

Table 16 Composition of colon stromal cell medium.

Reagent	Volume (per 1 ml medium)	Final concentration
Advanced DMEM/F-12	887 µL	-
Fetal bovine serum (FBS)	100 µL	10%
Penicillin/streptomycin	10 µL	100 U/mL
Y-27632	3 µL	10 µM

For BMP2 / GREM1 treatments, stromal cells were cultured with recombinant mouse proteins: 50 ng/mL rBMP2 and/or 500 ng/mL rGREM1 for five days, unless otherwise indicated.

To perform a conventional epithelium-stroma co-culture, 4x10^4 primary stromal cells were added to 2500 epithelial cells in a 10-µl Matrigel drop and cultured with organoid medium for 4 days prior to analysis.

2.2.3 Reconstitution of colon assembloids

Colon organoids aged 3-4 days were collected through physical pipetting with organoid harvesting solution and put on ice for 30 min. When the Matrigel was depolymerized completely, the intact organoids were washed gently with Advanced DMEM/F-12 and were allowed to settle by gravity (or centrifuging at 100 g for 1 min at 4 °C). The supernatant was removed, and the organoids were resuspended in Matrigel. The primary colon stromal cells cultured in 75-cm^2 flasks were treated with 5 mL TrypLE and incubated for 15 min at 37 °C. The dissociated cells were washed with Advanced DMEM/F-12 and centrifuged at 400 g for 5 min at 4 °C. The cell number was determined, and the cells were resuspended in Matrigel (1.5 x 10^5 cells per 3.5 µL Matrigel). After being sprayed with 70 % (vol/vol) ethanol, a sheet of Parafilm measuring 2.5 x 3 cm was placed in a 100-mm petri dish, with several drops of PBS placed around the Parafilm to maintain humidity. A 2-µL Matrigel droplet containing stromal cells was placed on the Parafilm using a P10 pipette. After that, 0.5 µL of organoids with 1.5 µl of stromal cells were immediately but slowly added into the droplet (4 µL Matrigel per assembloid in total). Ideally, organoids should be in the center of the droplet and the organoid number should be comparable. The petri dish containing six assembloids was covered with a lid and incubated at 37 °C for 10-15 min to solidify the gel. The assembloids were removed from the Parafilm using fine forceps and put into a 12-well plate (6-8 assembloids per well). Unless otherwise indicated, each well contained 1.5 mL of organoid medium without sWnt, CHIR-99021, R-spondin 1, and noggin. The plate was placed onto an orbital shaker at 120 rpm in the cell incubator. The assembloids were left to mature and were collected for further analyses after 4-5 days of shaking the culture, unless indicated otherwise. Mature assembloids can be passaged and reconstituted with fresh stromal cells.

To monitor assembloid growth, the epithelial cells from *tg Act-DsRed* mice were assembled with the stromal cells from *tg Act-CFP* mice. To visualize Axin2$^+$ cells and their immediate progeny, the assembloids were generated with epithelial cells from *Axin2CreERT2/Rosa26-tdTomato* mice and were treated with 1.5 µM 4OH-tamoxifen for 24 hours before collecting. *Bmpr1a* KO organoids were assembled with WT stromal cells to make epithelium-specific *Bmpr1a* KO (*Bmpr1a*$^{\triangle EPI}$) assembloids. To induce knock-out

of *Bmpr1a*, the stromal cells from *Bmpr1a*$^{fl/fl}$ mice were treated with 4 μM TAT-CRE Recombinase for 24 hours. The KO stromal cells were expanded, harvested, and assembled with WT organoids to make mesenchyme-specific *Bmpr1a* KO (*Bmpr1a*$^{\triangle MES}$) assembloids.

2.2.4 Reconstitution of colon tumor assembloids

To induce colitis-associated tumors, mice were administered intraperitoneal injections of 9.5 mg/kg azoxymethane (AOM). Five days later, mice received 2 % dextran sodium sulfate (DSS) in drinking water for a period of six days. Mice were monitored for three months before analyses. The colon was dissected and opened longitudinally for the assessment of tumors. To prepare the organoid culture, tumor tissue was dissected and incubated in TrypLE for 10 min at 37 °C. Cells were washed in 0.1 % BSA/PBS, seeded in basement membrane, and cultured with full organoid medium. sWnt and CHIR-99021 were withdrawn to select Wnt-independent organoids. The colon tumor assembloids were then generated with Wnt-independent organoids.

2.2.5 Single-cell RNA sequencing

The assembloids derived from two C57BL/6 mice were incubated in calcium and magnesium-free HBSS containing Liberase TL (1 unit/mL) and DNase I (1 unit/mL) at 37 °C for 1 hour, with pipetting every 10 min. Every 20 min, the digested fraction was collected and put into an ice-cold stromal cell medium containing Advanced DMEM/F12, 10 % FBS, 10 % penicillin/streptomycin, and 10 μM Y-27632. The collected fraction was filtered through a 70-μm cell strainer and centrifuged at 400 g for 5 min at 4 °C. Cell clusters were incubated with TrypLE for 5 min at 37 °C and filtered through a 40-μm cell strainer. Each sample was run with Chromium Single Cell kits, following the manufacturer's instructions.

A total of 16242 EpCAM-negative cells from assembloids were analyzed. Seurat v3 R package[68] was used for the whole pipeline, with a cut-off of at least 500 genes in a single cell and a maximum of 10 % mitochondrial reads. Normalization was carried out using the SCTransform function, including a mitochondrial percentage regression. Integration was performed with SCTransform to eliminate the batch effect of the two samples. A

t-distributed stochastic neighbor embedding (t-SNE) analysis was applied using the first 30 PCA dimensions. The Seurat FindClusters function was applied with a resolution of 0.1. For the dot plot presentation, the expression of genes in each cluster was represented as the average level of expression of those cells and the proportion of cells that express those genes. Cell-cell interactions were assessed with R package CellChat[69] using standard settings with at least 10 cells supporting each interaction.

2.2.6 Histology and imaging

Organoids/assembloids were transferred to 4 % paraformaldehyde (PFA) and fixed for 2 hours at room temperature (assembloids were fixed overnight at 4 °C), followed by incubation in 0.1 % BSA/PBS for at least 30 min, embedding in 2 % agarose, dehydration, and embedding in paraffin. 5-µm sections (prepared with HistoCore AUTOCUT microtome) were deparaffinized and rehydrated, followed by antigen retrieval in citrate buffer. A hydrophobic barrier was created with a Pap pen around the sections. Non-specific antibody binding was blocked by incubation in blocking buffer (0.1 % Tween/PBS [PBST] supplemented with 5 % FBS and 1 % BSA) for 1 hour, followed by overnight incubation with primary antibodies. The next day, they were washed with PBST, incubated with secondary antibodies (Alexa 488, Cy3, or Alexa 647) (1:250) for 2 hours at room temperature, and counterstained with DAPI (1:300). After staining, the sections were washed with PBST, mounted with Immu-Mount, and covered with cover glasses. For whole-mount staining of assembloids, the latter were fixed in 4 % PFA for 1 hour at room temperature, then washed with PBS followed by permeabilization in blocking buffer (PBS with 3 % BSA, 1 % saponin, and 1 % Triton X-100, 0.02 % Na Azide) overnight prior to staining. The staining procedure was the same as that for sections. After staining and washing, the assembloids were transferred to a microscope slide with a CoverWell imaging chamber, and mounted with VectaMount aqueous mounting medium.

Immunofluorescence imaging procedures were acquired with the Zeiss Observer 7 microscope and the confocal laser scanning microscope Leica TCS SP8. Live cell imaging was performed on the EVOS M5000 imaging system. Images were analyzed with Leica Application Suite X (LAS X), ZEN 3.4, ImageJ 2.0.0 (Fiji), and Imaris 9.8.

2.2.7 Tissue processing

The colon samples were placed in embedding cassettes, fixed with 4 % PFA solution for 24 hours at 4 °C, followed by washing with PBS. Samples were embedded in paraffin overnight using Logos One automat, cut into 5-µm thick sections, and stained with hematoxylin and eosin (H&E) by Anja Kuehl from Charité Core Unit Immunopathology for Experimental Models. Briefly, sections were dewaxed by incubation in two rounds of xylene for 2 min each time, 100 % ethanol for 1 min, 96 % ethanol for 1 min, 85 % ethanol for 1 min, 70 % ethanol for 1 min, and distilled water for 1 min. Then sections were stained with hematoxylin for 2 min, washed with tap water until the water turned clear, then stained with eosin for 1 min, followed by incubation in 70 % ethanol for 1 min, 85 % ethanol for 1 min, 96 % ethanol for 1 min, 100 % ethanol for 1 min, and two rounds of xylene for 2 min each time. After staining, the sections were covered with mounting medium (e.g., Histokitt).

2.2.8 Single-molecule RNA in situ hybridization

Assembloid/colon tissue sections measuring 5 µm in thickness were used for single-molecule in situ hybridization (sm-ISH) (SuperFrost Plus gold adhesion microscope slides were used for assembloids). RNAscope Red Detection Kit was used to detect the RNA in situ signal according to the manufacturer's protocol. Slides were baked in the HybEZ Oven at 60 °C for 1 hour and deparaffinizated by two rounds of xylene incubation for 5 min each time, followed by two rounds of incubation for 2 min each in 100 % ethanol. Samples were incubated with hydrogen peroxide at room temperature for 10 min. After washing in distilled water, samples were placed into boiled Target Retrieval Reagents and incubated at about 95 °C for 15 min. After target retrieval, samples were immediately washed with distilled water briefly, followed by incubation in 100 % ethanol for 3 min. ImmEdge pen was used to draw a hydrophobic barrier around the sections. On the next day, the samples were incubated with Protease Plus at 40 °C for 20 min for assembloids (30 min for colon tissue) and washed with distilled water. Hybridization with specific probes and amplification of the signal were performed with washing in Wash Buffer reagents after each incubation. Of note, probes needed to be prewarmed at 40 °C for 10 min before use. Samples were incubated with probes at 40 °C for 2 hours, then with AMP1 at

40 °C for 30 min, AMP2 for 15 min, AMP3 for 30 min, AMP4 for 15 min, AMP5 at room temperature for 45 min and, finally, AMP6 at room temperature for 15 minutes. Next, Fast Red-A and Fast Red-B reaction mix was used to incubate slides at room temperature for 10 min to detect the signal. Samples were then counterstained in 50 % hematoxylin for 2 min and 0.02 % ammonia water for 10 sec. After washing with distilled water, samples were baked in the HybEZ Oven at 60 °C for 20 min, dehydrated briefly with xylene, and covered with EcoMount mounting medium. Images of samples were obtained with the Zeiss Observer 7 microscope and analyzed with ImageJ 2.0.0 (Fiji).

2.2.9 Flow cytometry

The colon stromal cells were extracted from culture plates for $CD34^+$ cell proportion analysis after BMP2 treatment. Sub-clusters of cells were stained with antibodies against cell surface markers, including CD326 (EpCAM) PE (1:200), CD45 APC-Cy7 (1:200), CD31 APC (1:200), and CD34 FITC (1:100), and compensation control (UltraComp eBeads). Live/dead staining was performed by incubating cells with Fixable Viability Stain FVS450 (1:1000) according to the manufacturer's protocol. Flow cytometry experiments were performed on a Cytek Aurora 3-laser spectral cytometer. Data were analyzed with FCS Express 7 software.

For the experiment of BMP2 treatment of $CD34^+$ cells, stromal cells were isolated from mouse colon tissue as described above. Following appropriate antibody staining (CD326 (EpCAM) PE [1:200], CD45 APC-Cy7 [1:200], CD31 APC [1:200], CD34 FITC [1:100], FVS450 [1:1000]) and compensation control, samples were sorted into $CD34^+$ (live, $EpCAM^-$ $CD45^-$ $CD31^-$ $CD34^+$) or $CD34^-$ (live, $EpCAM^-$ $CD45^-$ $CD31^-$ $CD34^-$) populations in sterile condition using a FACS Aria III.

2.2.10 RNA isolation and qRT–PCR

Cell medium was removed following retrieval of cells from cultures, and RNA was isolated using the NucleoSpin RNA isolation kit according to the manufacturer's instructions. Measurement of the RNA concentration was performed with NanoDrop One Microvolume

UV/Visible Spectrophotometer. Complementary DNA (cDNA) was obtained with the iScript cDNA synthesis kit via reverse transcription with the PeqSTAR thermocycler. Related components are shown in Table 17 and reverse transcription was performed using the program shown in Table 18. cDNA was stored at -20 °C after reverse transcription.

Table 17 Components for reverse transcription reaction.

Name	Volume (per 20 µl)
RNA + DNase/RNase free water	15 µL (RNA: 500 ng)
5xiScript reaction Mix	4 µL
iScript reverse transcriptase	1 µL

Table 18 Reverse transcription program.

Time	Temperature
5 min	25 °C
21 min	46 °C
1min	95 °C
-	4 °C

qRT–PCR was performed using SYBR-green and the QuantStudio Real-Time PCR System. Primers for qRT-PCR analysis (Table 12) were validated by serial dilutions of RNA template, which was plotted against the threshold cycle (C_t) to create a standard curve. The qRT-PCR reaction mixture (Table 19) was prepared and added into a 96-well plate (15 µL/well).

Table 19 Components of qRT-PCR reaction mixture.

Name	Volume (per well)
SYBR green master mix	10 µL
Primer mix (forward + reverse primers)	1 µL
DNase/RNase free water	5 µL

cDNA was pipetted into the 96-well plate (5 µL/well) containing reaction mixture to ensure a total volume of 20 µL per well. The 96-well plate was covered with a film, centrifuged briefly, and put into the QuantStudio 3 Real-Time PCR System. The program for quantitative PCR is shown in Table 20.

Table 20 qRT-PCR program.

Stage	Step	Time	Temperature
Hold	Inactivation of RT and activation of Taq polymerase	10 min	95 °C
PCR (40 cycles)	Melting of double strands Primer annealing and elongation	15 sec 1 min	95 °C 60 °C
Melt curve	Denaturation Annealing denaturation	15 sec 1 min 15 sec	95 °C 60 °C 95 °C

For each primer pair and RNA sample, the reaction was done in technical duplicate. QuantStudio 3 Real-Time PCR Software v1.7.1 was applied to analyze amplification plots of qRT-PCR. The expression levels were quantified relatively calculating ΔC_t as well as $2^{-\Delta\Delta Ct}$ with glyceraldehyde-3-phosphate dehydrogenase (*Gapdh*) as an endogenous reference.

2.2.11 Statistical analysis

Data are expressed as mean ± SEM. A p-value of <0.05 was considered significant. The Mann-Whitney test (two-tailed) was applied to identify differences between the two groups. The Kruskal-Wallis test followed by a respective post-hoc analysis (Dunn's multiple comparisons test) was used for statistical comparison of more than two groups. No statistical methods were used to predetermine sample size. Data are displayed for independent biological samples, and at least two independent experiments were performed for the displayed datasets. GraphPad Prism 8 and RStudio1.4.1717 were used for data visualization and statistical analysis.

3 Results

3.1 Self-sufficient colon assembloids recapitulate *in vivo* epithelial crypt organization

To investigate the crosstalk between epithelium and stromal cells in the context of crypt development and homeostasis, I aimed to develop a co-culture system that includes both cell types. Simply adding primary stromal cells to epithelial cells in a drop of Matrigel did not lead to a clear pattern of interaction between these two cell types or *in vivo*-like morphology, as stromal cells tended to migrate out of the Matrigel and adhere to the bottom of the plate (Figure 4).

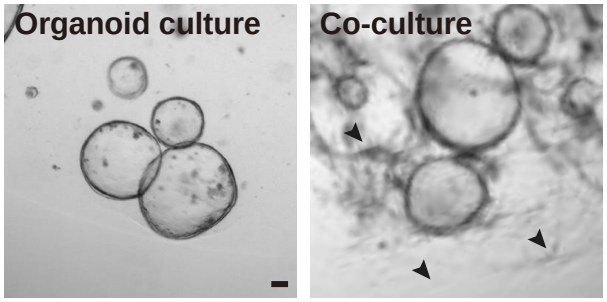

Figure 4 Conventional co-culture of colon organoids and stromal cells.

Colon organoids cultured with stromal cells did not show *in vivo*-like morphology. Scale bar: 100 µm.

To overcome this, I developed a two-step process to generate an assembloid co-culture model (Figure 5a-c). Using isolated murine colon crypts and stromal cells, I first generated three-dimensional (3D) epithelial organoids as well as primary stromal cell cultures as described previously[30,36] (Figure 5a). For assembly, I mixed the pre-cultured stromal cells into a drop of Matrigel and immediately added individual organoids into each droplet (Figure 5a, b). To maintain an even layer of stromal cells around the organoids and ensure equal access of the entire surface to the medium, the cultures were grown on an orbital shaker (Figure 5a, b).

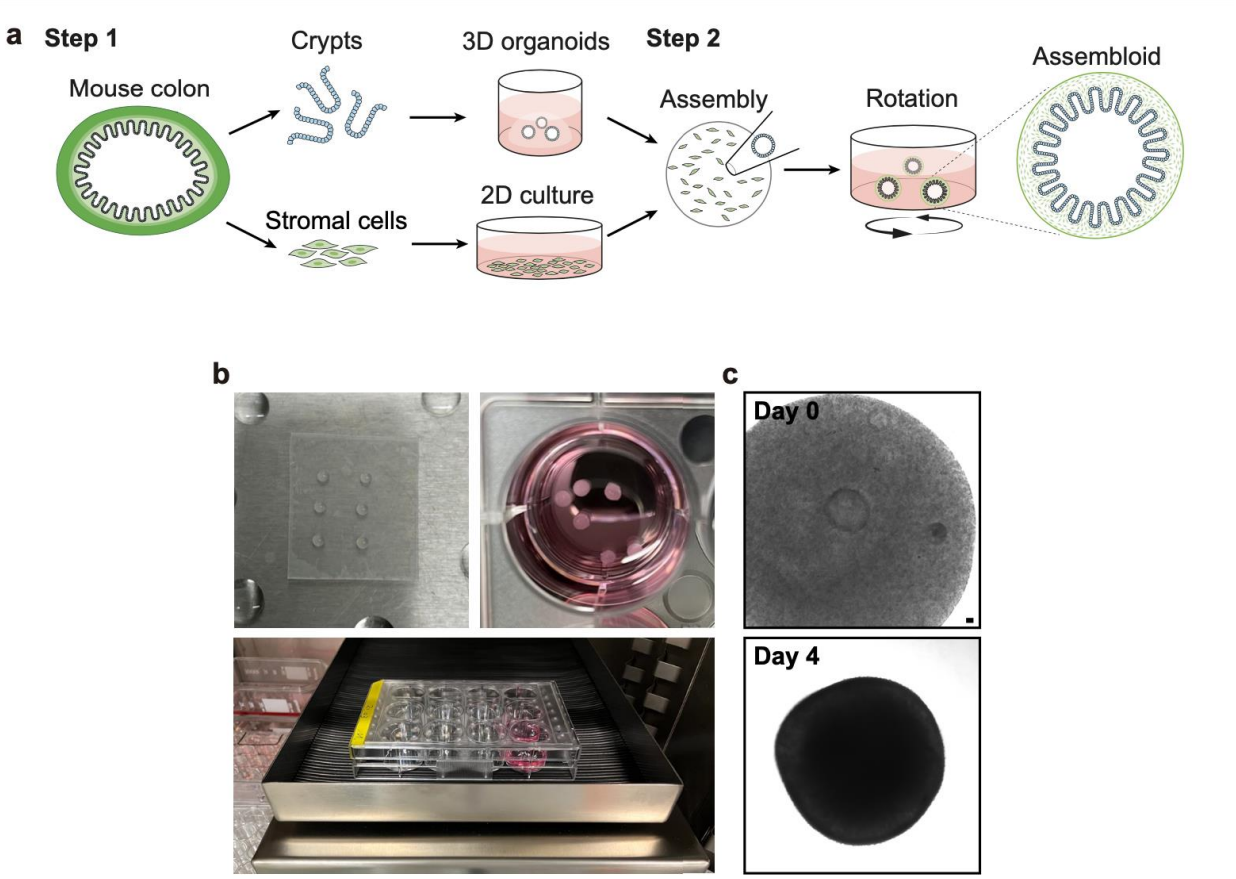

Figure 5 Schematic presentation and images of generating colon assembloids.

a) Step 1: Murine colon crypts and stromal cells were isolated and cultured separately. Step 2: Organoids and stromal cells were assembled and grown on an orbital shaker.

b) Upper left panel: Droplets of assembloids were placed on the Parafilm; upper right panel: assembloids were cultured in a 12-well plate; lower panel: the culture plate was placed on an orbital shaker.

c) Bright-field images of assembloids on day 0 and day 4. Scale bar: 100 µm.

To monitor the epithelium and stroma over time in the culture, I assembled DsRed-labeled organoids with CFP-labeled stromal cells derived from *tg Act-DsRed* and *tg Act-CFP* mice, and cultured them in full 3D organoid medium (FM). Using live-cell fluorescent imaging or whole-mount staining with confocal microscopy, I was able to follow the spatio-temporal growth of epithelial and stromal compartments (Figure 6a, b). Daily tracing of the assembloids demonstrated a fast expansion of the epithelial compartment (Figure 6a, b). At day 4 of the assembloid culture, the epithelia formed crypt-like structures surrounded by a tightly connected stromal layer (Figure 6c).

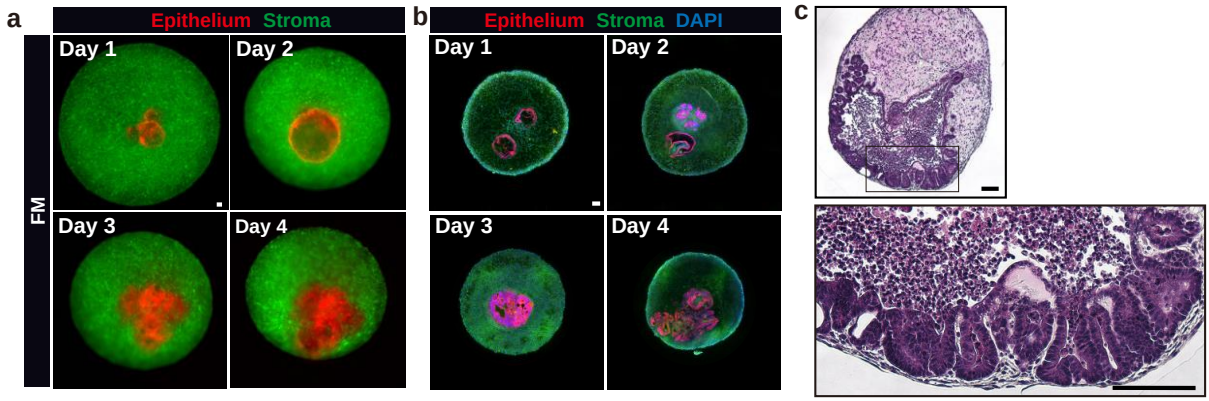

Figure 6 Colon assembloids grown in full medium (FM).

a) Live fluorescent images of assembloids cultured in FM for 1-4 days. The epithelium was derived from *tg Act-DsRed* mice, the stroma from *tg Act-CFP* mice. Scale bar: 100 µm.

b) Confocal microscopy images of whole-mount staining for assembloids cultured in FM for 1-4 days. The epithelium was derived from *tg Act-DsRed* mice, the stroma from *tg Act-CFP* mice. Scale bar: 100 µm.

c) H&E staining images of assembloids cultured in FM for 4 days. Scale bar: 100 µm.

Since stromal cells provide important niche factors for intestinal crypts *in vivo*[14], I asked myself whether epithelial crypt formation could be induced by factors produced by the stromal cells alone. Therefore, I removed Wnt activators (Wnt [W], CHIR-99021 [C], R-spondin [R]) and the BMP inhibitor noggin (N) (WCRN) from the culture medium, which are normally required for stem cell maintenance in organoid cultures[36,37,39]. Despite the absence of such critical factors, I found that epithelial expansion in assembloids grown in WCRN-free (-WCRN) medium leads to the formation of crypt-like structures comparable to those formed in FM (Figure 7a, b). Since the supplementation of growth factors was dispensable, I employed the WCRN-free medium for all subsequent experiments in the current study.

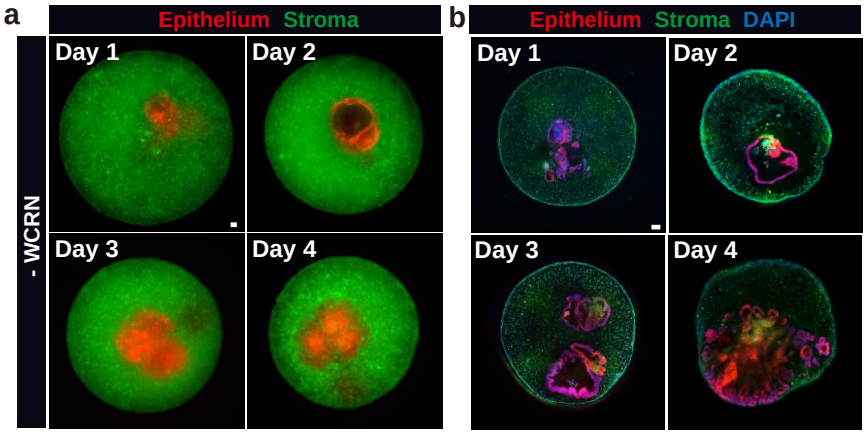

Figure 7 Colon assembloids grown in medium without sWnt, R-spondin1, CHIR99021, and noggin (-WCRN).

a) Live fluorescent images of assembloids cultured in -WCRN medium for 1-4 days. The epithelium was derived from *tg Act-DsRed* mice, the stroma from *tg Act-CFP* mice. Scale bar: 100 µm.

b) Confocal microscopy images of whole-mount staining for assembloids cultured in -WCRN medium for 1-4 days. The epithelium was derived from *tg Act-DsRed* mice, the stroma from *tg Act-CFP* mice. Scale bar: 100 µm.

I performed a time-course experiment to observe crypt formation in assembloids grown in -WCRN medium for 1 to 4 days (Figure 8a). On day 1, the epithelium in assembloids presented as a monolayer forming a simple cyst-like structure (Figure 8a). This was followed by epithelial cell thickening and polarized organization of stromal cells in parallel to the epithelial lining one day later (Figure 8a). On day 3, I observed multiple epithelial invaginations with migration of stromal cells into the space between them, followed by a formation of true crypts on day 4 (Figure 8a).

In vivo, colonic stem cells require high Wnt signaling activity, which is highest at the crypt bottom and induces the expression of the bona fide Wnt target gene Axin2[28,39,70]. To visualize Wnt-activated stem cells over time, I applied *Axin2CreErt2/Rosa26-tdTomato* lineage-tracing mice, as described before[13,28], to generate assembloids grown for 1 to 4 days, and treated them with tamoxifen for 24 h to induce tdTomato expression in Axin2-expressing cells (Figure 8b). I found that tdTomato$^+$ cells were spread over the epithelium on day 1, while the proportion of positive cell islets was reduced with epithelial expansion one day later (Figure 8b). On day 3, tdTomato$^+$ cells began to concentrate in the lower

part of invaginations and ultimately stayed at the base of each crypt in assembloids on day 4 (Figure 8b). My findings showed a dynamic change of Wnt signaling activity during assembloid maturation and an *in vivo*-like Axin2$^+$ cell distribution in mature epithelia of assembloids cultured without supplementation of Wnt-inducing factors.

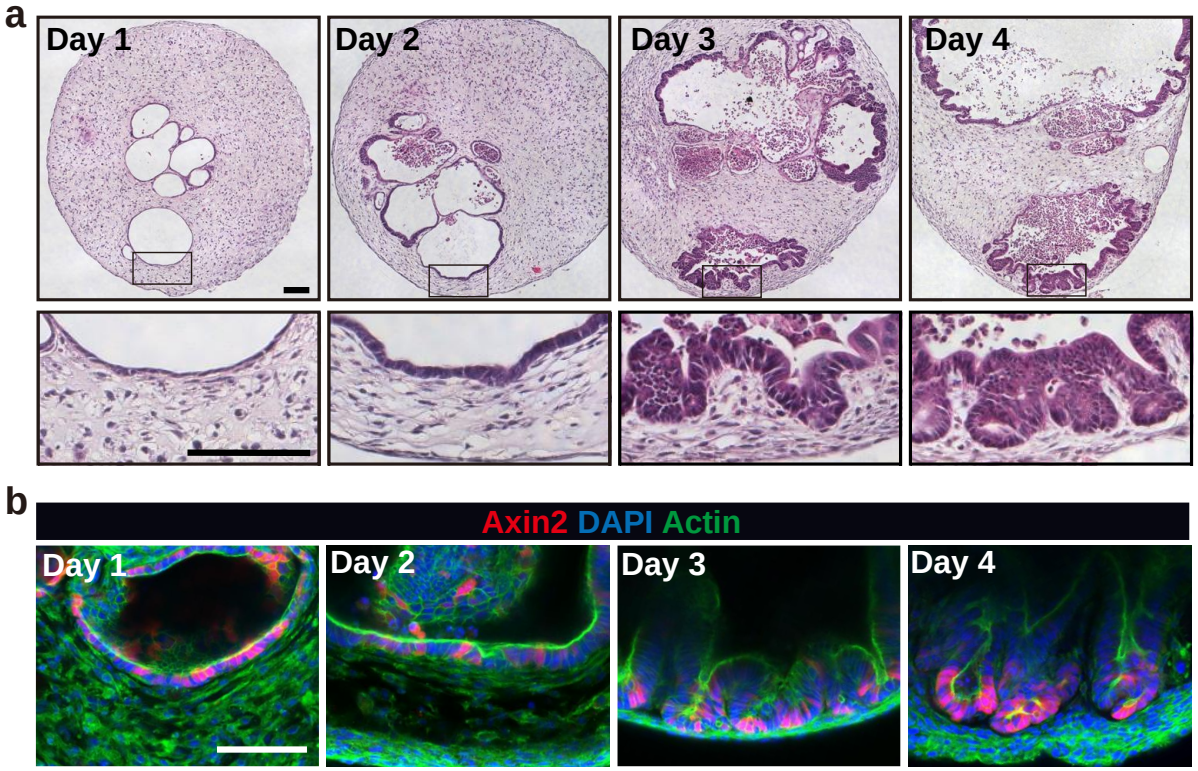

Figure 8 Cellular organization and Axin2$^+$ cell distribution during assembloid maturation.

a) H&E staining images of assembloids cultured in medium without sWnt, CHIR99021, R-spondin1, and noggin (-WCRN) for 1-4 days. Scale bar: 100 µm.

b) Confocal microscopy images of whole-mount staining for assembloids (cultured in -WCRN medium) derived from *Axin2CreERT2/Rosa26-tdTomato* mice, cultured in -WCRN medium for 1-4 days, showing Axin2 lineage tracing for 24 h. Scale bar: 100 µm.

Yap1 is a transcriptional regulator that is largely inactive in the epithelium during homeostasis but becomes active during development and is re-induced by injury, whereupon it drives a “fetal-like” regeneration process[71-73]. Using immunofluorescence labeling, I observed that in sections of adult mouse colon, active Yap1 was indeed only present at low levels, whereas it was highly expressed in the nuclei of organoids grown in FM, indicating that organoids resemble regenerative epithelium (Figure 9a). Notably, assembloids also had high nuclear levels of active Yap1 at early stages on days 1 and 2, before being shut

down on days 3 and 4, as crypts formed (Figure 9b). These results demonstrate that assembloids mimic the crypt maturation from “fetal-like” regenerative cells to normal adult crypts.

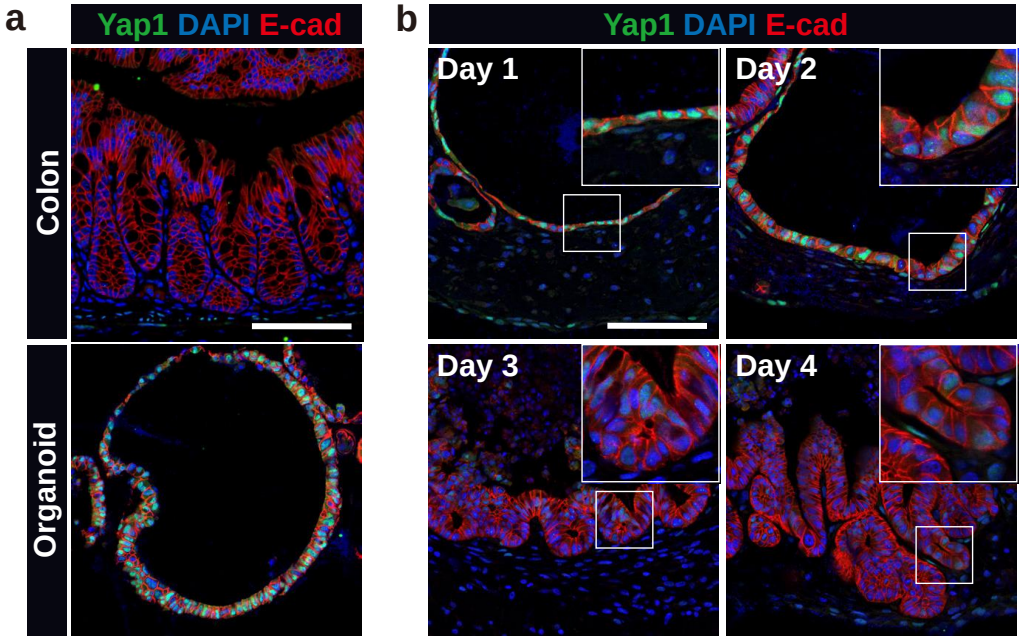

Figure 9 Active Yap1 staining for the colon, organoids, and assembloids.

a) Immunofluorescence images of the colon and organoids stained for active Yap1. Scale bar: 100 µm.

b) Immunofluorescence images of colon assembloids cultured in -WCRN medium for 1-4 days stained for active Yap1. Scale bar: 100 µm.

To further explore how closely assembloids resemble the native tissue, I compared crypts in colon tissue with those in assembloids (Figure 10). I found a similar cellular crypt organization, with cell proliferation restricted to the lower part of the crypts, as assessed by Ki67 staining (Figure 10, left), while Krt20-expressing differentiated surface enterocytes were located in the upper part (Figure 10, second from left). In addition, numerous Muc2^{+} goblet cells and synaptophysin (Syp)$^{+}$ enteroendocrine cells were identified in the assembloids, resembling *in-vivo* crypts (Figure 10). High-resolution imaging of enterocytes, goblet cells, and enteroendocrine cells in the assembloids revealed that they appeared fully differentiated and closely resembled the morphology of these cell types *in vivo* (see magnifications in Figure 10).

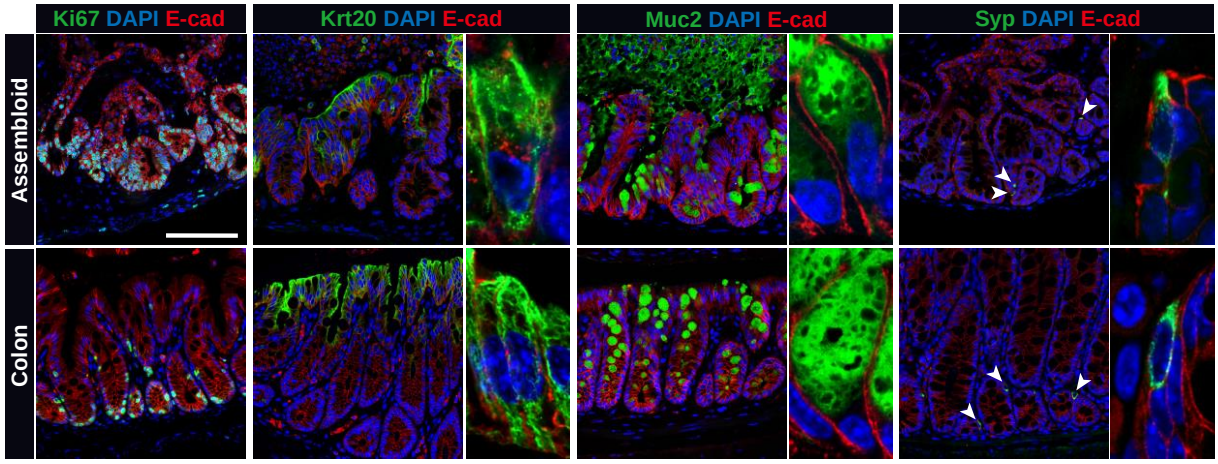

Figure 10 Epithelial cell organization in assembloids compared to *in vivo* crypts.

Immunofluorescence images of colon assembloids (grown in -WCRN medium) and colon tissue stained for proliferative cells (Ki67), enterocytes (Krt20), goblet cells (Muc2), and enteroendocrine cells (Syp). Scale bar: 100 µm.

Notably, this cellular self-organization could not be achieved in colonic organoids: Most cells in organoids grown in FM were highly proliferative ($Ki67^+$), while differentiated cells such as $Krt20^+$ enterocytes and $Muc2^+$ goblet cells were rarely observed (Figure 11). While differentiation of organoids can easily be achieved by removing growth factors from the medium[39], this approach enriches differentiated cells at the expense of proliferation and stemness (Figure 11), such that organoids represent a rather binary setting – either stemness or differentiation. Taken together, these results demonstrate that colon epithelia grown as assembloids rebuild and faithfully mimic the epithelial cellular architecture and cell-type composition of the native tissue.

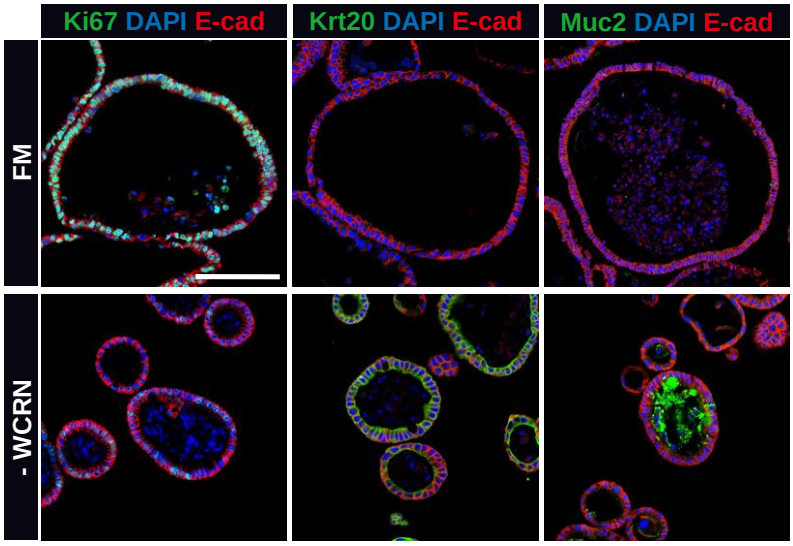

Figure 11 Colon organoids require additional sWnt, CHIR99021, R-spondin1, and noggin (WCRN) for proper cell turnover.

Immunofluorescence images of colon organoids cultured in full medium (FM) or -WCRN medium, stained for proliferative cells (Ki67), enterocytes (Krt20), and goblet cells (Muc2). Scale bar: 100 µm.

3.2 Stromal cellular diversity in colon assembloids

The thus obtained data indicated that stromal cells are a determinant of epithelial crypt formation and cellular organization. To shed light on the cellular diversity in the stroma of colon assembloids, single-cell RNA sequencing (scRNA-seq) from assembloids were performed and cataloged 16,242 non-epithelial cells (EpCAM-negative) for further analysis. Graph-based clustering revealed six distinct cell clusters (Figure 12a, b, scRNA-seq analyses performed in collaboration with Hao Li): two distinct fibroblast-like stromal cell populations stromal 1 and 2 (both expressing fibroblast markers such as *Col1a2* and *Pdgfra*), myofibroblasts (*Acta2* high), neurons (*Elavl4*$^+$), glial cells (*S100b*$^+$), and endothelial cells (*Pecam1*$^+$). I visualized endothelial cells in assembloids by immunofluorescence and identified CD31$^+$ endothelial cells similar to those found in the colon tissue (Figure 12c). I used β3-tubulin (Tubb3) to identify neuronal cells that were distributed throughout the stroma compartment as observed in the colon (Figure 12c). Vimentin (Vim)$^+$ fibroblasts were located beneath and between crypts in close contact with the epithelium, whereas

α-SMA$^+$ myofibroblasts were found mainly in the outer layer, similar to the lamina muscularis mucosae in the colon (Figure 12d).

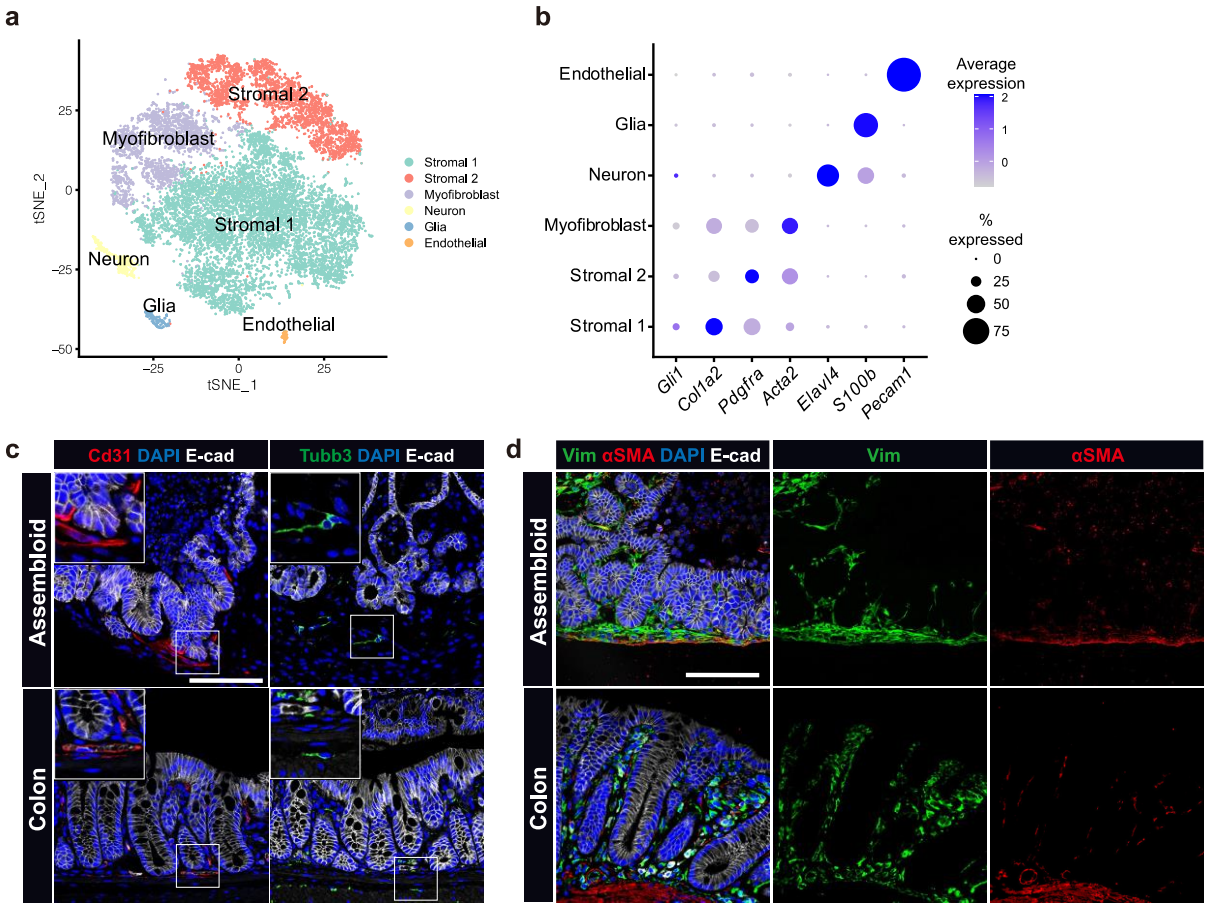

Figure 12 Mesenchymal cellular complexity in colon assembloids.

a) t-SNE plot of the scRNA-seq dataset from colon assembloid stromal cells.

b) Dot plot showing the expression of known marker genes against stromal cell clusters identified by scRNA-seq. The circle size represents the within-cluster probability of gene detection. The fill color represents the normalized average expression level.

c) Immunofluorescence images of colon assembloids and colon tissue stained for endothelial cells (Cd31) and neural cells (Tubb3). Scale bar: 100 µm.

d) Immunofluorescence images of colon assembloids and colon tissue stained for fibroblasts (Vim) and myofibroblasts (αSMA). Scale bar: 100 µm.

To understand the intercellular communication networks in the stromal compartment in assembloids, we performed a CellChat analysis and found that there were numerous signaling crosstalks among stromal cell clusters, including Collagen and Laminin pathways (Figure 12a, b, CellChat analysis performed by Hilmar Berger), both of which are critical

for maintaining the extracellular matrix and supporting stem cell survival[74,75]. Of note, Stromal 2 was the main resource of BMP ligands that were sensed by Stromal 2 itself and other cell clusters (Figure 12b).

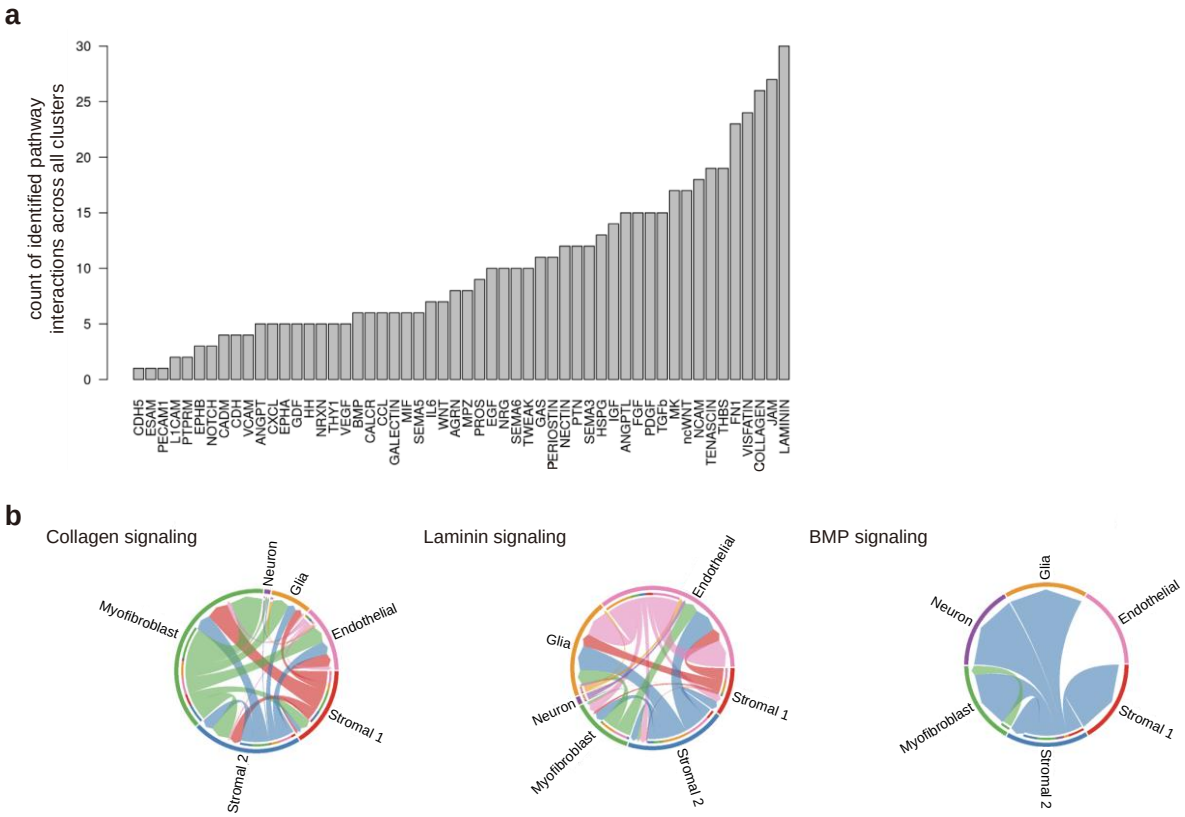

Figure 13 Intercellular communication networks in the stromal compartment in assembloids.

a) Identified pathway interactions across stromal clusters.

b) Collagen, laminin, and BMP signaling interactions across stromal clusters.

Based on the expression of the marker genes *Cd34*, *Cd81* and *Foxl1*[12,29,30,76] I identified the stromal cell population 1 as trophocytes (*Cd34*$^{+}$ *Cd81*$^{+}$ *Foxl1*$^{-}$) and the stromal cell population 2 as telocytes (*Cd34*$^{-}$ *Cd81*$^{-}$ *Foxl1*$^{+}$) (Figure 14a). Stromal 1 was also marked by the Wnt agonist *Rspo3* (Figure 14a, c), a key driver of stem cell turnover[13,77], while stromal 2 expressed high levels of the non-canonical Wnt ligand *Wnt5a*, and periostin (*Postn*) (Figure 14a, c), which is in line with previous *in-vivo* findings[12,29]. Of note, Wnt5a and Postn were shown to be critical for epithelial homeostasis and tissue repair[78,79]. I assessed the spatial distribution of the two mesenchymal populations in assembloids using single-molecule in situ hybridization (sm-ISH) for *Foxl1* and *Rspo3* (Figure 14b). *Foxl1*

expression (stromal 2/telocytes) was located primarily along the crypt axis with only a few cells in close proximity to the epithelium at the crypt base. *Rspo3* expression detecting trophocytes (stromal 1) was confined to beneath the crypts. Overall, these data demonstrate that assembloids imitate not only the epithelial but also the mesenchymal architecture of colonic crypts *in vivo* to a great extent, recapitulating the diversity and spatial distribution of stromal cells including telocytes and trophocytes.

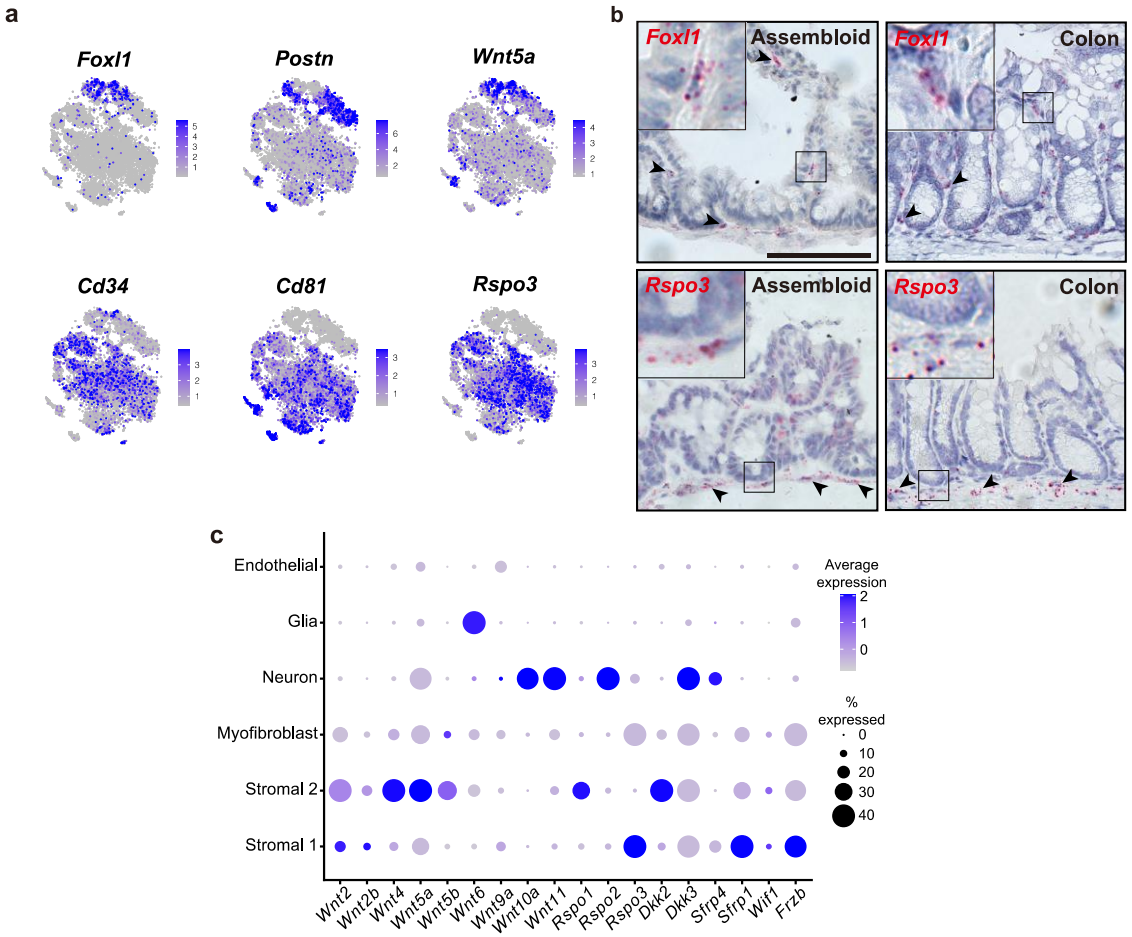

Figure 14 Subsets of stromal fibroblasts in assembloids.

a) t-SNE expression plots of telocyte marker genes (*Foxl1*, *Postn*, and *Wnt5a*) and trophocyte marker genes (*Cd34*, *Cd81*, and *Rspo3*) in the assembloid dataset. Cells colored by normalized expression of indicated marker genes.

b) Single-molecule in situ hybridization (sm-ISH) showing the localization of *Foxl1* and *Rspo3* in assembloids and the colon tissue. Scale bar: 100 µm.

c) Dot plot showing the expression of Wnt signaling molecules in identified clusters.

3.3 BMP signaling is spatially organized in colon assembloids

Telocytes and trophocytes are decisive for the epithelial hierarchical organization of the crypt as they express molecules with opposing effects on BMP signaling[29]. To explore the functionality of the identified telocytes and trophocytes in assembloids, I assessed the expression of factors that regulate BMP signaling. The BMP antagonists *Grem1*, *Grem2*, and *Mgp* were expressed in the stromal 1 population, while the BMP agonists *Bmp2*, *Bmp5*, and *Bmp7*, were almost exclusively expressed in stromal 2 (Figure 15a, b). sm-ISH of assembloids and colon tissue sections revealed expression of *Bmp2* predominantly at the top of crypts in both epithelial and stromal cells, gradually decreasing towards the base, before disappearing completely in the stem cell compartment (Figure 15c). The spatial distribution of the BMP inhibitor *Grem1*, which was previously shown to be a specific trophocyte marker[29], was present in subcryptal stromal cells in colon tissue, and expression was also concentrated in this compartment in assembloids (Figure 15c). These findings suggest that assembloids have functional telocytes and trophocytes that orchestrate a gradient of BMP signaling molecules along the crypt axis.

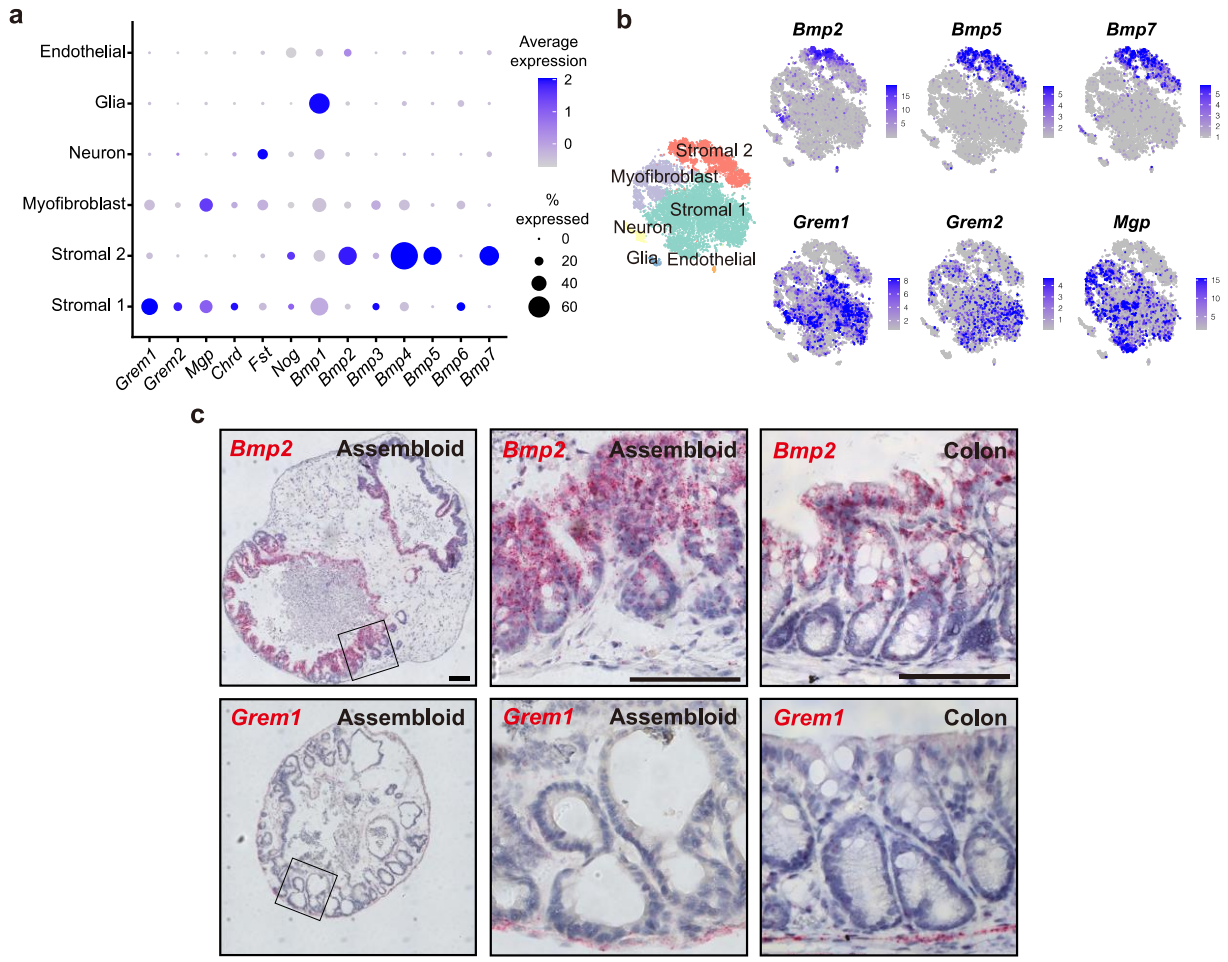

Figure 15 BMP gradient in colon assembloids.

a) Dot plot showing the expression of BMP signaling molecules in identified clusters.

b) t-SNE expression plots of BMP ligand genes (*Bmp2*, *Bmp5*, and *Bmp7*) and Bmp antagonist genes (*Grem1*, *Grem2*, and *Mgp*).

c) sm-ISH showing the localization of *Bmp2* and *Grem1* in assembloids and colon tissue. Scale bar: 100 µm.

3.4 BMP signaling drives crypt formation

BMP is established as a factor that drives cell differentiation in the gastrointestinal tract[43]. Standard colon organoids exposed to varying concentrations of recombinant BMP2 display pronounced growth inhibition (Figure 16a). qPCR revealed an increased expression of the BMP target gene *Id1* and the differentiation marker *Krt20* in response to a BMP concentration gradient. In contrast, the stem cell marker *Lgr5* was already strongly downregulated by a low dose of BMP2 (5 ng/mL) (Figure 16b). Notably, the endogenous *Bmp2*

expression was strongly upregulated by BMP2 (Figure 16b). This is consistent with our previous findings in the stomach which showed a positive feed-forward loop of BMP signaling in epithelial cells triggered by intercellular signaling from the stroma[80].

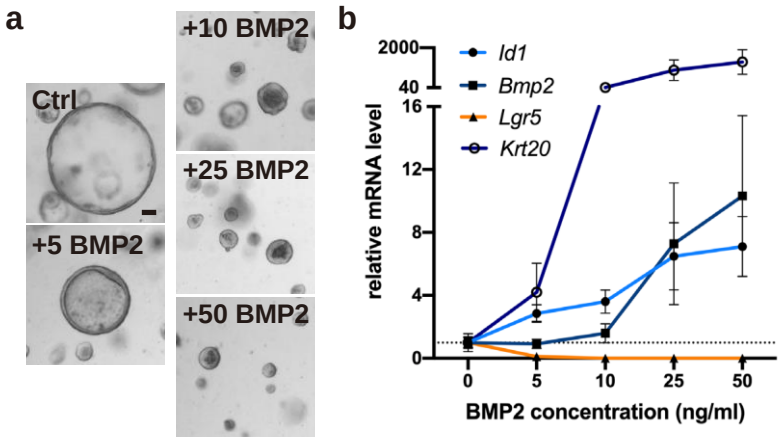

Figure 16 BMP2 gradient treatment of colon organoids.

a) Representative images of colon organoids cultured in full medium (FM) or exposed to the indicated BMP2 concentrations (without noggin). Scale bar: 100 µm.

b) qPCR for *Lgr5*, *Krt20*, *Bmp2*, and *Id1* from organoids cultured in the indicated conditions (*n*=3).

sm-ISH analysis showed that *Bmp2* was expressed in differentiated surface cells in the colon *in vivo* as well as in our assembloids (Figure 15c). To address whether unspecified and differentiated colon epithelial cells exhibit differences in *Bmp2* expression, I differentiated organoids by removing the growth factor cocktail WCRN, which maintains stemness, thereby inducing growth inhibition and cell differentiation (Figure 17a, 11). This was validated by a strongly reduced expression of the stem cell marker *Lgr5* and upregulation of the enterocyte marker *Krt20* at the mRNA level (Figure 17b). Organoids in -WCRN medium showed an almost 10-fold increased expression of endogenous *Bmp2*, concomitant with an upregulation of *Id1* (Figure 17b), indicating that cells that exit the stem cell niche initiate *Bmp2* expression even without exposure to BMP ligands. Taken together, my data support the hypothesis that exposure of epithelial cells to the stem cell niche inhibits epithelial Bmp2 expression, while cells that migrate out of the stem cell niche induce Bmp2 expression, which is further augmented via a feed-forward loop to enforce cellular differentiation.

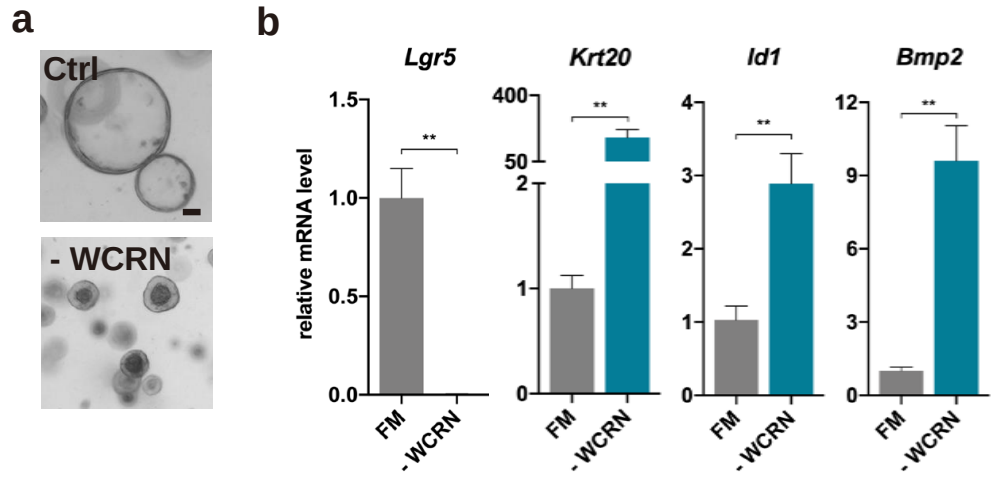

Figure 17 Differentiated colon epithelial cells induce Bmp2 expression.

a) Representative images of colon organoids cultured in full medium (FM) or medium without sWnt, CHIR99021, R-spndin1, and noggin (-WCRN). Scale bar: 100 µm.

b) qPCR for *Lgr5*, *Krt20*, *Bmp2*, and *Id1* from organoids cultured in the indicated conditions (n=6). Data are presented as mean ± SEM. Statistical analyses were performed using the Mann-Whitney test (two-tailed). *p < 0.05, **p < 0.01, ***p < 0.001, ****p < 0.0001.

I took advantage of the assembloid culture technique to explore the role of BMP signaling in establishing crypt cell organization. To this end, I generated genetically heterogeneous assembloids with wild-type (WT) stromal cells and BMP type I receptor *Bmpr1a* KO epithelial cells (*Bmpr1a*$^{\Delta EPI}$) that were derived from *Axin2CreErt2/Bmpr1a*$^{fl/fl}$ mice. I found that assembloids containing *Bmpr1a* KO epithelial cells failed to compartmentalize, with the epithelium remaining organized in a flat monolayer (Figure 18a). In addition to the defective crypt formation, epithelial cells also failed to differentiate, as assessed by the expression of Krt20 and Muc2 (Figure 18b). In contrast, the pan-proliferative marker Ki67 was expressed throughout the epithelium. Overall, these results demonstrate that induction of BMP signaling in epithelial cells is essential for cell specification and crypt formation.

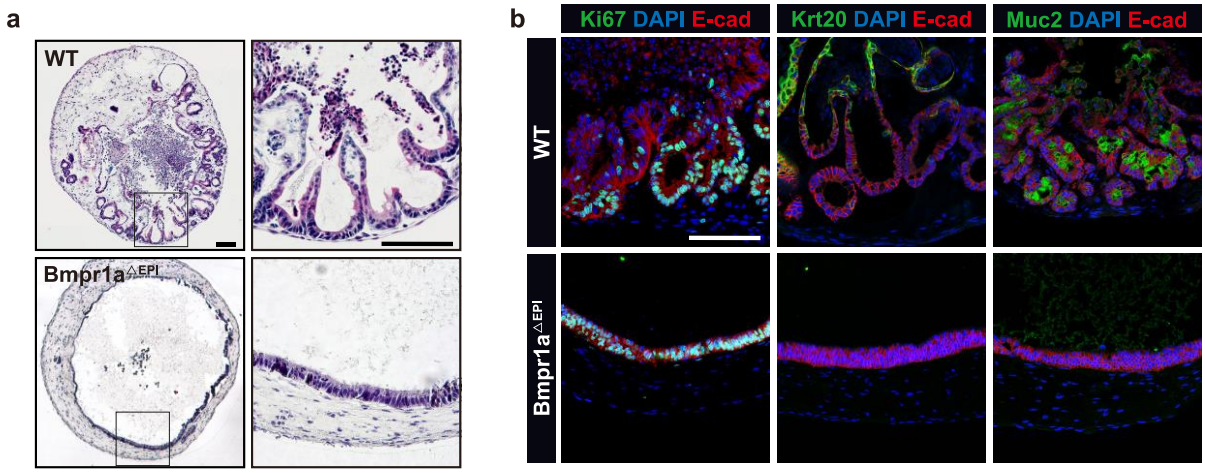

Figure 18 Epithelium-specific *Bmpr1a* knock-out assembloids.

a) H&E staining images of the assembloid derived from wild-type mice (WT) and the assembloid comprising epithelial cells from *Axin2CreErt2/Bmpr1a*$^{fl/fl}$ mice (*Bmpr1a*$^{\triangle EPI}$). Scale bar: 100 µm.

b) Immunofluorescence images of WT and *Bmpr1a*$^{\triangle EPI}$ assembloids stained for Ki67, Krt20, and Muc2. Scale bar: 100 µm.

3.5 BMP signaling modulates stromal cell functions

As indicated above, the stromal compartment is an important reservoir of BMP signaling molecules[29,81]. However, whether and how BMP signaling also affects this compartment itself is less clear. To investigate this, I generated assembloids with *Bmpr1a* KO stromal cells and WT epithelial cells (*Bmpr1a*$^{\triangle MES}$). Strikingly, the epithelial cells again failed to compartmentalize and crypt structures emerged only rarely and focally (Figure 19a). Similarly to the *Bmpr1a*$^{\triangle EPI}$ assembloids, most epithelial cells of the *Bmpr1a*$^{\triangle MES}$ assembloids remained proliferative and failed to differentiate (Figure 19b). These findings suggest that crypt generation also requires activation of BMP signaling in the stroma.

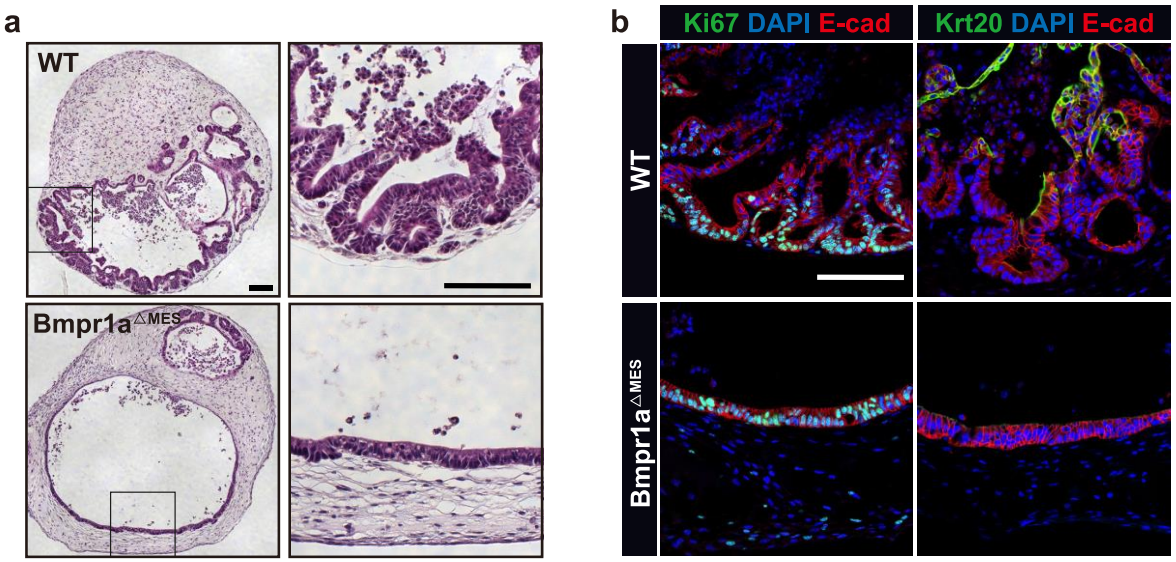

Figure 19 Stroma-specific *Bmpr1a* knock-out assembloids.

a) H&E staining images of the wild-type (WT) assembloid and the assembloid comprising *Bmpr1a* KO stromal cells derived from *Bmpr1a*$^{fl/fl}$ mice (*Bmpr1a*$^{\triangle MES}$). Scale bar: 100 µm.

b) Immunofluorescence images of WT and *Bmpr1a*$^{\triangle MES}$ assembloids stained for Ki67 and Krt20. Scale bar: 100 µm.

To study the impact of BMP signaling on mesenchymal stromal cells, I treated primary colon stromal cells with BMP2. qPCR confirmed their responsiveness by an upregulated expression of *Id1* after BMP2 treatment (Figure 20). I noticed that, similar to the epithelium, BMP2 also triggered the expression of *Bmp2* (Figure 20). Given that Bmp2 is expressed mainly in telocytes, but not in trophocytes in assembloids, which is consistent with *in-vivo* data[14], I wondered whether Bmp2 induces telocyte-like features. Remarkably, I found that the telocyte markers *Foxl1* and *Wnt5a* were both increased, while the trophocyte markers *Cd34* and *Grem1* were downregulated after rBMP2 treatment (Figure 20). These effects could be reversed by adding the BMP inhibitor GREM1 to the culture (Figure 20), which in turn resulted in an increased expression of *Grem1* (Figure 20).

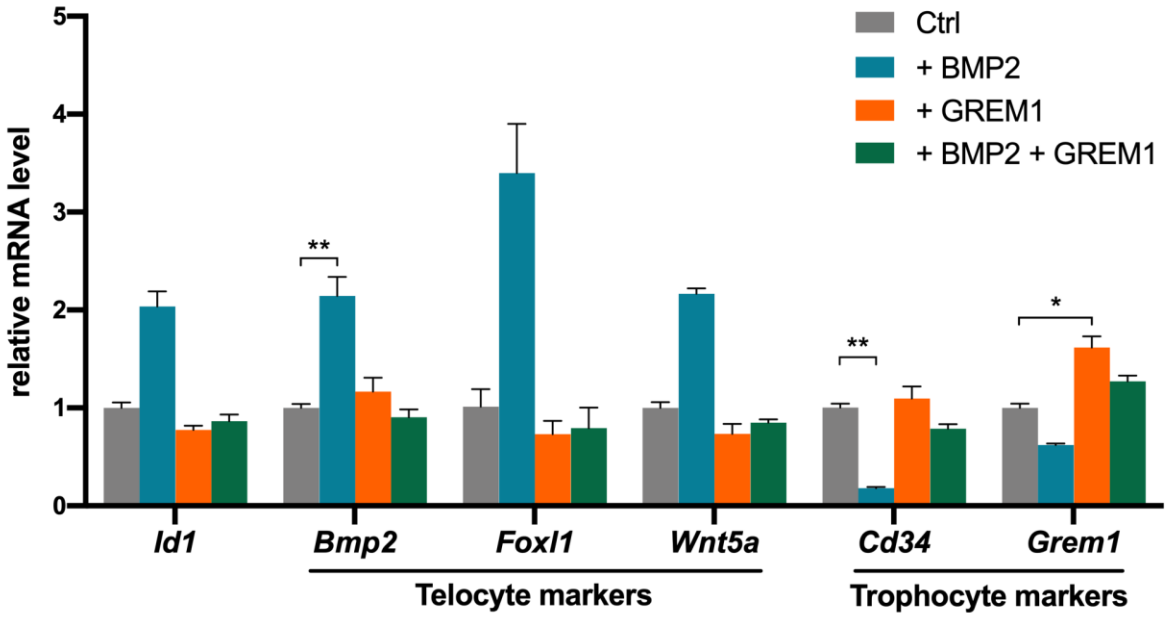

Figure 20 BMP2 and GREM1 treatment of primary colon stromal cells.

qPCR for BMP target gene *Id1*, telocyte marker genes (*Bmp2*, *Foxl1*, and *Wnt5a*), trophocyte marker genes (*Cd34* and *Grem1*) of primary murine colon stromal cells cultured in normal medium, or treated with 50 ng/mL BMP2, 500 ng/mL GREM1, or 50 ng/mL BMP2 and 500 ng/mL GREM1 (n=6). Data are presented as mean ± SEM. Statistical analyses were performed using the Kruskal-Wallis test, followed by Dunn's multiple comparisons test. *p < 0.05, **p < 0.01, ***p < 0.001, ****p < 0.0001.

Flow cytometry of stromal cells treated with BMP2 revealed a remarkable reduction in the proportion of $EpCAM^-$ $CD45^-$ $CD31^-$ (non-epithelial, non-immune, non-endothelial) $CD34^+$ stromal cells (Figure 21a, b; experiment performed in collaboration with Kimberly Hartl) in the culture, indicating that BMP induces a loss of the trophocyte-like cell population. Thus, my data suggest that the spatial organization of niche cells along the crypt axis is driven by BMP signaling: Surface epithelial cell-derived Bmp2 induces differentiation into telocyte-like cells that themselves express Bmp2, thereby further stabilizing BMP signaling. The base, by contrast, is characterized by a lack of BMP signaling, sustained by stromal expression of BMP inhibitors.

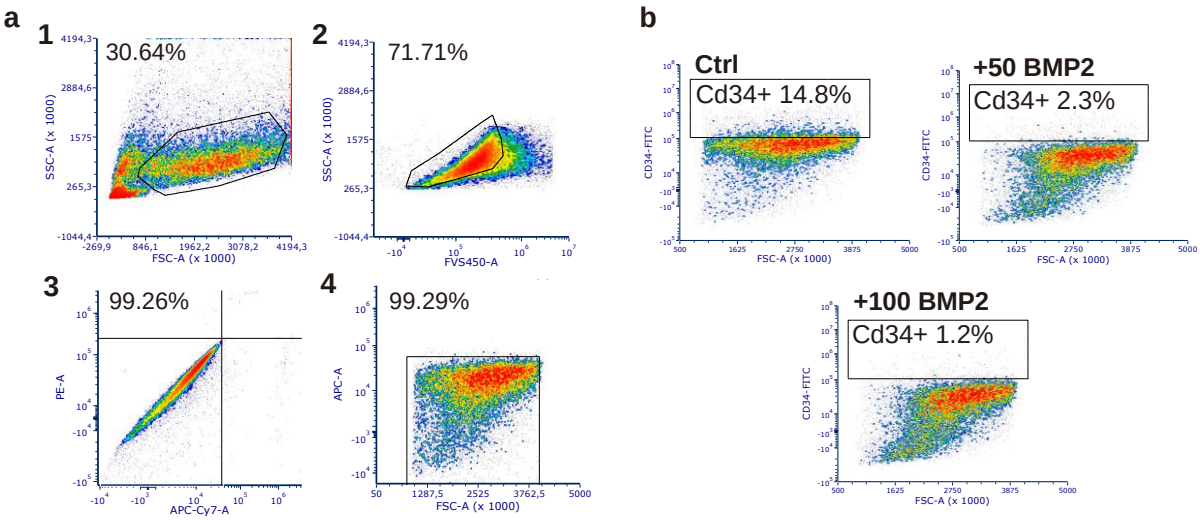

Figure 21 Flow cytometry analysis for CD34$^+$ cells from BMP2 treated primary stromal cells.

a) Representative flow cytometry gating strategies for analyses of alive (FVS450$^-$) EpCAM (PE)$^-$ CD45 (APC-Cy7)$^-$ CD31 (APC)$^-$ primary murine colonic stromal subsets. Cells were gated with forward and sideward scatter (FSV-A and SSC-A) (panel 1), and dead cells were excluded by staining and gating for negative cells with FVS450 (panel 2). Immune cells and epithelial cells were excluded by gating the double negative population (CD45 (APC-Cy7)$^-$/EpCAM (PE)$^-$) (panel 3). Finally, endothelial cells were excluded by gating for CD31 (APC)-negative cells (panel 4).

b) Flow cytometry analysis of the EpCAM$^-$ CD45$^-$ CD31$^-$ CD34 (FITC)$^+$ cell proportion in primary murine colon stromal cells cultured in normal medium or treated with the indicated BMP2 concentrations.

To further examine the effect of Bmp2 on trophocytes, fluorescence-activated single-cell sorting (FACS) was performed to isolate EpCAM$^-$ CD45$^-$ CD31$^-$ CD34$^+$ stromal cells from murine colon and exposed them to different concentrations of BMP2 (Figure 22a; experiment performed in collaboration with Kimberly Hartl). qPCR showed that BMP2 promoted a concentration-dependent decrease of trophocyte gene expression, including *Cd34*, *Rspo3*, *Grem1*, and *Mgp*, while the expression of telocyte marker genes was increased (Figure 22b). Together, these results demonstrate that BMP signaling determines the functional state of stromal cells, allowing a functional transition from a trophocyte- to a telocyte-like state upon exposure to Bmp2.

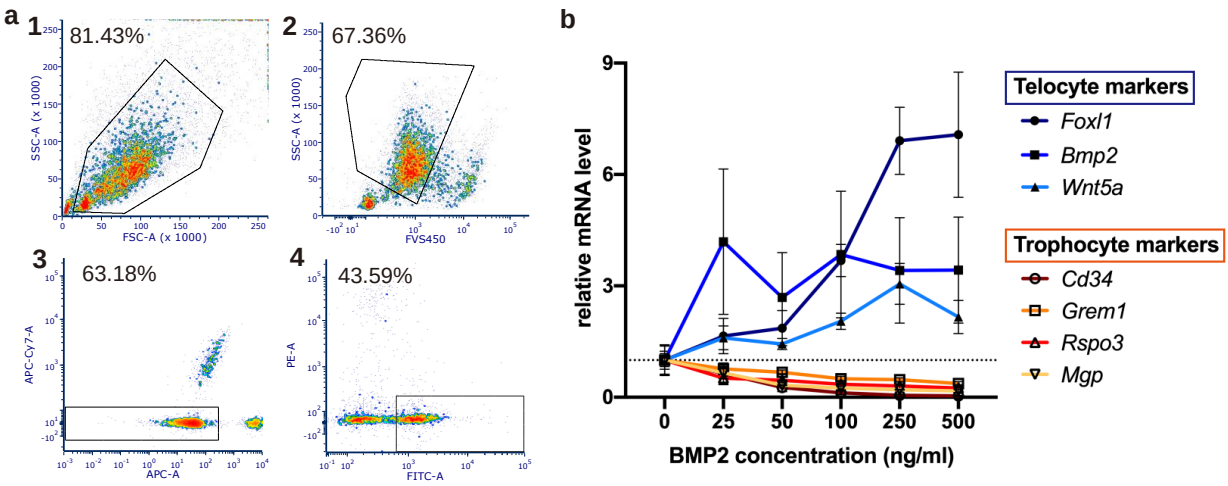

Figure 22 Impact of BMP2 on CD34$^+$ stromal cells.

a) Representative FACS gating strategies for sorting EpCAM$^-$ CD45$^-$ CD31$^-$ CD34$^+$ murine stromal cells. Cells were gated with forward and sideward scatter (FSV-A and SSC-A) (panel 1), and dead cells were excluded by staining and gating for negative cells with FVS450 (panel 2). Immune cells and endothelial cells were excluded by gating the double negative population (CD45 (APC-Cy7)$^-$/CD31 (APC)$^-$) (panel 3). Finally, stromal cells were sorted by gating for the EpCAM (PE)$^-$/CD34 (FITC)$^+$ population (panel 4).

b) qPCR for telocyte marker genes (*Bmp2*, *Foxl1*, and *Wnt5a*), trophocyte marker genes (*Cd34*, *Grem1*, *Rspo3*, and *Mgp*) of EpCAM$^-$ CD45$^-$ CD31$^-$ CD34$^+$ primary murine colon stromal cells exposed to the indicated BMP2 concentrations (*n*=3).

3.6 Creation of colon tumor assembloids

To investigate whether assembloids can also be used to model intestinal tumorigenesis, we induced colitis-associated tumors in mice using the previously established azoxymethane (AOM) / dextran sodium sulfate (DSS) model (Figure 23a, this experiment was performed by Julian Heuberger)[82]. Organoids from the tumor tissue were grown and found that they exhibited Wnt-independent growth (Figure 23b, this experiment was performed by Julian Heuberger).

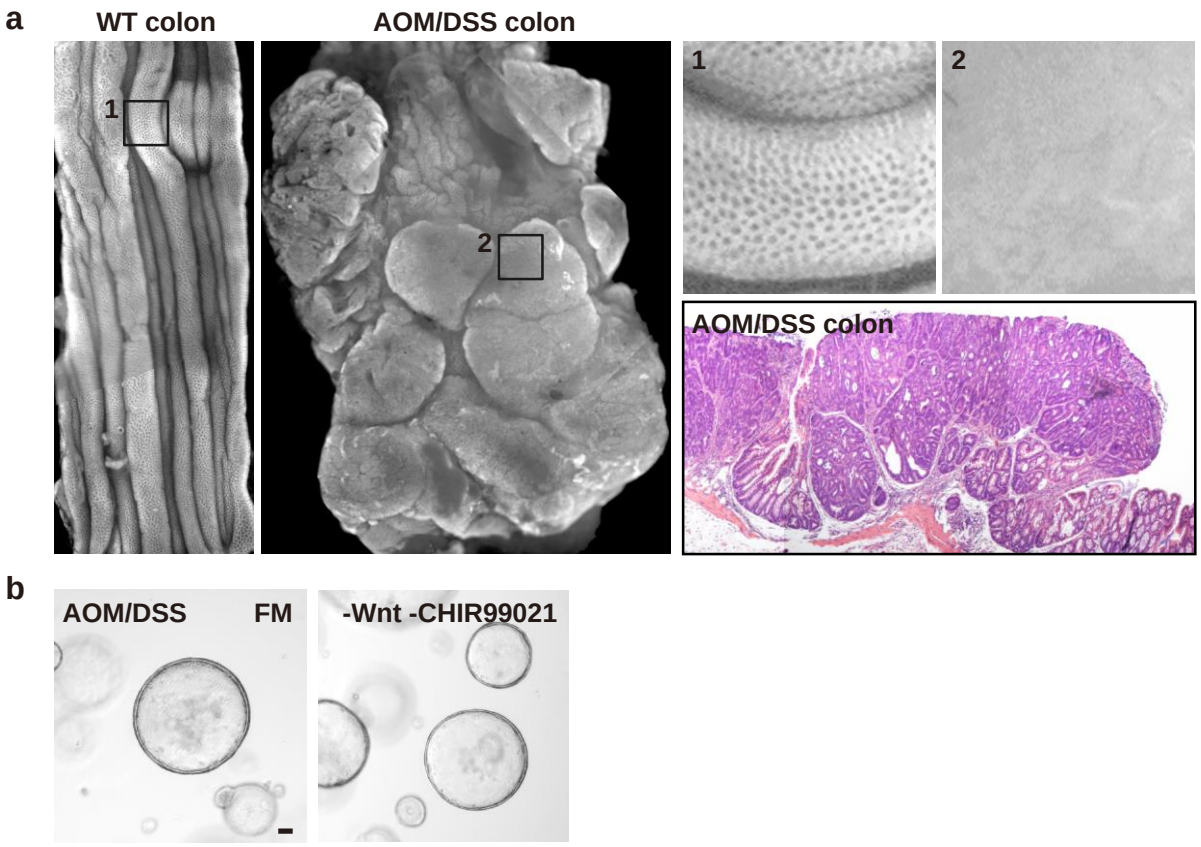

Figure 23 Establishment of AOM/DSS colitis-associated tumor model.

a) Representative images of wild-type (WT) colon tissue and AOM/DSS colon tumor tissue. (Images obtained from Julian Heuberger.)

b) Representative images of AOM/DSS tumor organoids cultured in full medium (FM), or medium without sWnt and CHIR99021. Scale bar: 100 µm. (Images obtained from Julian Heuberger.)

I then generated tumor assembloids using the Wnt-independent organoids and wild-type stromal cells. Colon tumor cells in assembloids grew as irregular ridges rather than typical crypt-like structures (Figure 24a), similarly to the tumor morphology *in vivo,* which I did not see when I cultured tumors as organoids (Figure 23b). Like the tumor cells *in vivo*, most epithelial cells in the assembloids were highly proliferative, and differentiation into colonocytes or goblet cells was impaired (Figure 24b). Interestingly, I noticed active nuclear Yap1 in both tumor assembloids and the tissue (Figure 24c), indicating a more primitive state with fetal-like properties[83]. Overall, these results confirm that the assembloid model is also able to accurately capture the morphological characteristics of colon tumors, suggesting that assembloids are a valuable tool for studying tumor biology and testing targeted interventions.

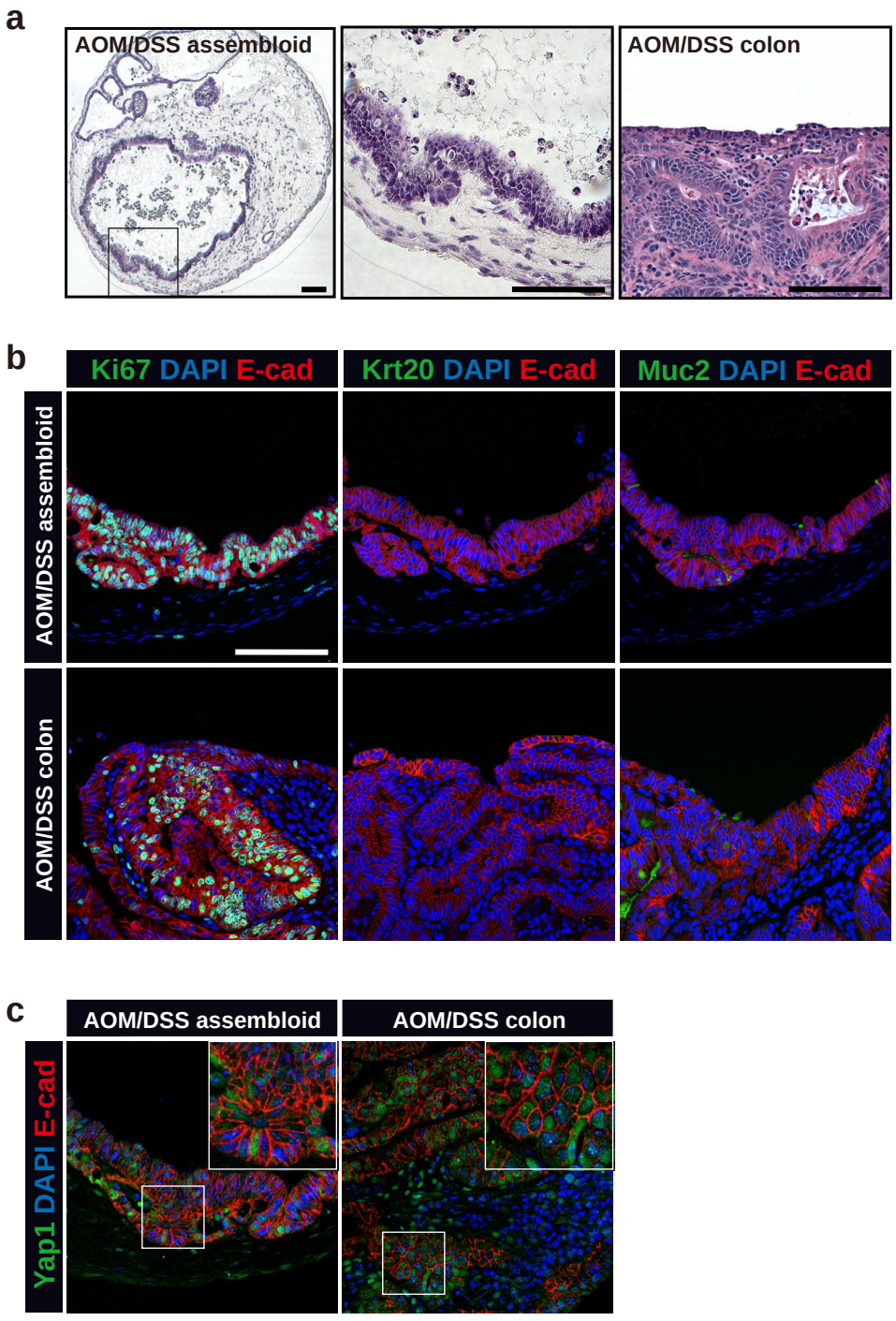

Figure 24 Generation of colon tumor assembloids.

a) H&E staining images of the colon tumor assembloid and the colon tumor tissue derived from AOM/DSS mouse model. Scale bar: 100 µm.

b) Immunofluorescence images of the tumor assembloid and the tumor tissue stained for Ki67, Krt20, and Muc2. Scale bar: 100 µm.

c) Immunofluorescence images of the tumor assembloid and the colon tumor stained for active Yap1. Scale bar: 100 µm.

4 Discussion

In this study I developed an assembloid culture system that enables the study of intercellular communication and self-organization of gastrointestinal tissues. By combining different cell types that can be isolated from different lines, the system lends itself to straightforward genetic modification of specific subsets of cells, which allowed me to dissect the molecular signals provided by stromal cells along the crypt axis that control epithelial proliferation and differentiation. The resulting data reveal a close interplay between the epithelium and the mesenchymal stroma during the process of crypt maturation, and provide information on key principles of regulation and mucosal homeostasis. My findings show that the epithelium shapes its own niche and that it is the reciprocal communication between the epithelium and the stroma that serves as the basis for homeostasis (Figure 25). By recapitulating the processes that coordinate epithelial self-organization and maturation, this system enables the investigation of gastrointestinal mucosal development and homeostasis *in vitro*, and will drive a better understanding of processes responsible for tissue dysfunction and malignant transformation.

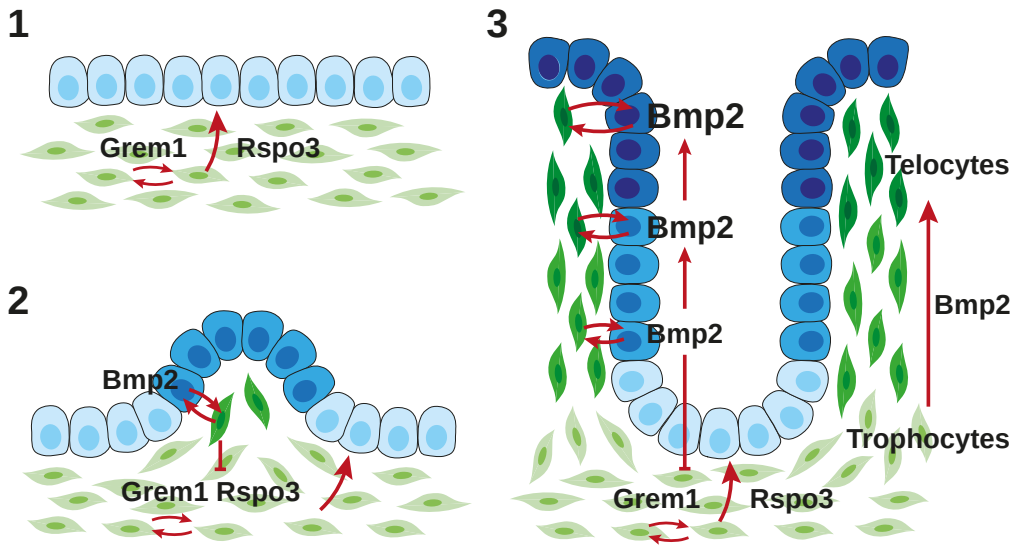

Figure 25 Schematic representation of the cellular interplay during crypt formation.

1) Stem cells are maintained by growth factors derived from trophocytes, such as Grem1 and Rspo3. Grem1 augments its own expression and thus stabilizes the stem cell niche.

2) With epithelial expansion a state is reached where the epithelium begins to fold and cells that are more distant from the stem cell niche initiate Bmp2 production. This shifts the BMP signaling in the stroma and allows a functional transition of stromal cells from a trophocyte- to a telocyte-like state;
3) Telocytes in turn also produce Bmp2 and, via this paracrine feed-forward loop of Bmp2 between the epithelium and the stroma, they further boost epithelial differentiation, compartmentalize telocytes and trophocytes, and ensure proper crypt formation.

4.1 Gastrointestinal cell culture systems

Currently, gastrointestinal organoids represent the standard for studying epithelial stem cell behavior in the gastrointestinal tract[84]. The organoid system has revolutionized biomedical research and also lends itself to the modeling of gastrointestinal disorders[33,40]. Organoids even mimic intestinal epithelial self-organization to a certain degree[35]. However, they mostly resemble the crypt base stem cell compartment[36]. Although differentiation can be induced by withdrawal of growth factors, the differentiation capacity of organoids is limited, and the stem cell compartment is lost in differentiation conditions, thus preventing the modeling of true homeostasis. This holds true particularly for colon organoids, which rely on high Wnt supplementation in contrast to organoids from the small intestine, resulting in a highly proliferative epithelium[36]. The assembloid system enables the generation of a culture that resembles mature crypts and contains both adult stem cells as well as differentiated cells, which I find to be a result of a reciprocal interplay between the stroma and the epithelium in the establishment of gastrointestinal crypts. Assembloids thus anatomically resemble the *in-vivo* state more closely and comprehensively than conventional organoid technology.

The high proliferative activity of the epithelium in the gastrointestinal tract makes it challenging to establish an ideal culture condition that includes less proliferative cells from the stroma. My data indicate that it is the absence of the stromal compartment that prevents colon organoids from faithfully replicating the cellular and morphological complexity of the epithelium *in vivo*. Recently, several groups have used co-culture systems with defined gastrointestinal cell subsets such as epithelial cells and fibroblasts/myofibroblasts[85,86], vessels[87], immune cells[88], or neural cells[89,90] derived from adult primary stem cells or pluripotent stem cells. These systems used either air-liquid interface (ALI) cultures where

stromal cells were separated from the epithelium or relied on the traditional organoid technique, with the additional cell types added to the static Matrigel drop. Both approaches have provided important insights but are unable to fully recapitulate the interplay between the epithelium and the stroma or the emergence of mature crypts *in vitro*. My system allows the expansion of epithelial cells in direct contact with the stromal cells and I was able to show that this close interplay is a crucial foundation for crypt maturation and the corresponding organization of the stroma.

A previous study reported the generation of assembloids from the urinary bladder as well as corresponding tumors[91]. These multilayer assembloids also exhibited characteristics of the mature adult tissue and elucidated the determination of tumor plasticity induced by stromal cells. However, unlike my colon assembloids, the stromal compartment of the bladder assembloid system was derived from heterologous origins, including mouse embryonic fibroblasts and the human lung microvascular endothelial cell line-5a (HULEC-5a). These cell lines indeed also supported the formation of organotypic structures by the epithelium. In my assembloid system, I used primary stromal cells from homologous tissue and was able to demonstrate the remarkable anatomical self-organization of these cells as well the underlying signals. Notably, primary stromal cells in my culture provide the Wnt activators and BMP inhibitors necessary for maintaining colon stem cells, making the colon assembloids self-sufficient with regards to these essential signaling pathways.

4.2 Trophocytes and telocytes

The subepithelial mesenchyme consists of distinct stromal cell types and forms a stem cell niche maintaining epithelial homeostasis[14]. Previous studies showed that the gastrointestinal stromal cells play a critical role during *H. pylori* infections and colitis[13,28,92]. The stromal cells respond to inflammation and injury, augment expression of key growth factors, such as Wnt agonist Rspo3 and BMP antagonist Grem1, and therefore promote epithelial regeneration[13,92]. Recently, several studies identified specific stromal cell subpopulations that are pivotal for epithelial homeostasis[30,31,93]. Degirmenci et al. showed that GLI1$^+$ stromal cells form critical Wnt-producing niches for colonic stem cell renewal[93]. Stzepourginski et al. suggested that pericryptal Cd34$^+$ stromal cells are a major component of the intestinal stem cell niche[30]. Cd34$^+$ cells that produce Wnt2b, Rspo1, and

Grem1 are rapidly activated by DSS colitis, augmenting Grem1 and Rspo1 as well as key factors that are important for the immunity of gastrointestinal tract and tissue repair, such as IL-7, Ccl2, and Ptgs2[30]. Upon intestinal injury, a subcluster of intestinal mesenchymal cells, named MAP3K2-regulated intestinal stromal cells (MRISCs), were described as being the main source of Rspo1[31]. Using single-cell RNA sequencing and fine-resolution microscopy, Kinchen et al. and McCarthy et al. provided a coherent view of stromal fibroblast clusters, such as trophocytes and telocytes[12,29]. These two subsets of fibroblasts regulate epithelial cell proliferation and differentiation by generating BMP and Wnt signaling gradients[12,29,30]. Trophocytes enrich underneath crypts and produce mainly BMP antagonists and Rspo3 to drive stem cell replication[12,29,30]. In contrast, BMP ligands and non-canonical Wnts expressed in telocytes that are distributed along crypts inhibit epithelial proliferation but promote differentiation[12,29,30].

The colon assembloids show functional and organized stromal cell populations, including stromal 1 and stromal 2, resembling trophocytes and telocytes *in vivo*. The molecular, anatomical, and functional properties of these two stromal cell types are becoming increasingly appreciated. However, the relationship between trophocytes and telocytes remains unclear. My data suggest that stromal cells are able to switch their functional state from trophocytes to telocytes in response to BMP signals from the differentiating epithelium. At the same time, the BMPs produced by telocytes further boost epithelial differentiation. Through this bidirectional communication between the epithelium and the mesenchyme, telocytes and trophocytes become compartmentalized and in turn maintain proper epithelial cell turnover and differentiation.

4.3 The impact of BMP signaling on cell organization

BMP signaling is required for epithelial cell differentiation in the gastrointestinal tract[43]. BMP drives rapid terminal differentiation of stem cells into Muc5ac$^+$ mucus pit cells in the stomach[80]. In the intestine, BMP signaling gradients control enteroendocrine cell specialization, as well as zonation of goblet cells and enterocytes[57,94]. In this study I demonstrated that not only the critical BMP ligand Bmp2 triggers its own expression in both colonic epithelium and stroma, but that the BMP inhibitor Grem1 augments its own expression as well. These two feed-forward loops of BMP signaling shape and stabilize the

polarized crypt architecture with its two distinct compartments: the proliferative base and the differentiated surface.

Previous studies have indicated that a deficiency of BMP signaling in the gastrointestinal epithelium or mesenchyme leads to pathological mucosal alterations[47,48,58-60,95,96]. In the stomach, deletion of *Bmpr1a* or overexpression of noggin promotes cell proliferation with increased numbers of chief cells, while the numbers of parietal cells are decreased[95,96]. Upon blocking BMP signaling, the intestinal epithelium shows abnormal hyperproliferation, formation of ectopic crypt units, and induces polyposis with an elevated cancer risk[48,58-60]. Deficiency of *Bmpr1a* in the intestinal stroma expands the stromal cell compartment, promotes the infiltration of immune cells, and alters extracellular matrix proteins, cytokines, and chemokines, eventually leading to polyposis induction[47]. Interestingly, an impaired crypt architecture and development of cyst-like aberrant structures within the colonic epithelium are found in most mouse models applied by these studies. These structures were also present in our *Bmpr1a*$^{\triangle EPI}$ and *Bmpr1a*$^{\triangle MES}$ assembloids, indicating that BMP signaling plays a significant role in proper crypt formation, and its absence induces premalignant pathologies. Apart from BMP, several molecular players that I observed to be regulated in the stroma by BMP, including Foxl1 and Wnt5a, are also involved in the emergence of intestinal crypts/villi during fetal development or wound healing[78,97-99], suggesting that BMP signaling orchestrates intercellular communication in the crypt.

4.4 Colon tumor model

Tumor formation involves both neoplastic epithelial cells and the complex microenvironment including the stroma[100]. Tumor development is not determined solely by genetic mutations in tumor cells, but also by the heterogeneity within cell types of the tumor microenvironment[100]. The interaction between tumor cells and the stroma shapes the tumor microenvironment and eventually supports tumor progression[100]. It has been shown that fibroblasts within the tumor exhibit augmented proliferation, extracellular matrix production, and cytokine secretion, which leads to extensive tissue remodeling[101]. The remodeled tumor microenvironment actively affects therapeutic response and resistance and therefore results in a poor prognosis for several types of cancer[102,103]. The fact that the

assembloid technique can capture several pathophysiological characteristics of colon tumors, including abnormal morphology, enhanced proliferation, and impaired differentiation, makes this technique very appealing. The reconstitution of tumor cells and stromal cells allows the model to better replicate the complexity of the tumor ecosystem, which is essential for improving the development of therapeutic strategies, especially for drug-resistant tumors. Further studies are needed to explore how tumor epithelial cells and stromal cells influence each other in assembloids, and how this interaction affects tumor development.

4.5 Future prospects

The incorporation of stromal cells into assembloids will enable insights into the interplay between the epithelium and the stroma in the context of injury and malignant transformation. Furthermore, I found that colon assembloids comprise cell types of the enteric nervous system and endothelium, which are also critical for gut homeostasis[16,104]. The assembloid system will enable the further exploration of their function, maturation, and interplay with other cell types. The current colon assembloid lacks an immune compartment that manipulates the development of inflammatory and malignant disorders. The addition of immune cells will enable the study of specific immune cells for homeostasis and gastrointestinal pathology. Notably, my system allows a rapid and simple cell-type-specific knockout of genes in defined subsets of cells, allowing simple and rapid validation of genetic alterations and perturbations of signaling pathways in either the epithelium or the stroma. The current assembloid model has been created only with murine colonic cells. Further investigation of the feasibility of the assembloid model in other organs as well as in human cells will be important.

5 Conclusions

Taken together, my results demonstrate that the colon assembloid system resembles the colonic crypt structure, including its key characteristic features such as stem cell organization, turnover, differentiation, and formation of signaling gradients along the crypt axis. Crypt formation is orchestrated by a bidirectional communication between the epithelium and the surrounding mesenchymal stroma. My findings reveal that the epithelium is not only controlled by the surrounding niche, but that it also shapes its own niche, resulting in a spatially and functionally highly organized microenvironment. I identified BMP signaling as a crucial signal that, in addition to driving epithelial differentiation, serves as a key signal in shaping the niche. Activation of BMP signaling promotes a functional switch in stromal cells from trophocyte-like stem cell niche cells to telocyte-like cells that produce several mediators which in turn promote differentiation. The assembloid system is thus suitable for modeling the complex interplay of epithelium and stroma in the gut and enabled us to identify key principles of mucosal self-organization.

References

1 Rao, J. N. & Wang, J. Y. in *Regulation of Gastrointestinal Mucosal Growth Integrated Systems Physiology: from Molecule to Function to Disease* (2010).

2 Barker, N., van Es, J. H., Kuipers, J., Kujala, P., van den Born, M., Cozijnsen, M., Haegebarth, A., Korving, J., Begthel, H., Peters, P. J. & Clevers, H. Identification of stem cells in small intestine and colon by marker gene Lgr5. *Nature* **449**, 1003-1007, doi:10.1038/nature06196 (2007).

3 van der Flier, L. G. & Clevers, H. Stem cells, self-renewal, and differentiation in the intestinal epithelium. *Annu Rev Physiol* **71**, 241-260, doi:10.1146/annurev.physiol.010908.163145 (2009).

4 Parikh, K., Antanaviciute, A., Fawkner-Corbett, D., Jagielowicz, M., Aulicino, A., Lagerholm, C., Davis, S., Kinchen, J., Chen, H. H., Alham, N. K., Ashley, N., Johnson, E., Hublitz, P., Bao, L., Lukomska, J., Andev, R. S., Bjorklund, E., Kessler, B. M., Fischer, R., Goldin, R., Koohy, H. & Simmons, A. Colonic epithelial cell diversity in health and inflammatory bowel disease. *Nature* **567**, 49-55, doi:10.1038/s41586-019-0992-y (2019).

5 Wang, Y., Song, W., Wang, J., Wang, T., Xiong, X., Qi, Z., Fu, W., Yang, X. & Chen, Y. G. Single-cell transcriptome analysis reveals differential nutrient absorption functions in human intestine. *J Exp Med* **217**, doi:10.1084/jem.20191130 (2020).

6 Kim, Y. S. & Ho, S. B. Intestinal goblet cells and mucins in health and disease: recent insights and progress. *Curr Gastroenterol Rep* **12**, 319-330, doi:10.1007/s11894-010-0131-2 (2010).

7 Johansson, M. E., Phillipson, M., Petersson, J., Velcich, A., Holm, L. & Hansson, G. C. The inner of the two Muc2 mucin-dependent mucus layers in colon is devoid of bacteria. *Proc Natl Acad Sci U S A* **105**, 15064-15069, doi:10.1073/pnas.0803124105 (2008).

8 Okumura, R. & Takeda, K. Roles of intestinal epithelial cells in the maintenance of gut homeostasis. *Exp Mol Med* **49**, e338, doi:10.1038/emm.2017.20 (2017).

9 Sternini, C., Anselmi, L. & Rozengurt, E. Enteroendocrine cells: a site of 'taste' in gastrointestinal chemosensing. *Curr Opin Endocrinol Diabetes Obes* **15**, 73-78, doi:10.1097/MED.0b013e3282f43a73 (2008).

10 Peterson, L. W. & Artis, D. Intestinal epithelial cells: regulators of barrier function and immune homeostasis. *Nat Rev Immunol* **14**, 141-153, doi:10.1038/nri3608 (2014).

11 Banerjee, A., McKinley, E. T., von Moltke, J., Coffey, R. J. & Lau, K. S. Interpreting heterogeneity in intestinal tuft cell structure and function. *J Clin Invest* **128**, 1711-1719, doi:10.1172/JCI120330 (2018).

12 Kinchen, J., Chen, H. H., Parikh, K., Antanaviciute, A., Jagielowicz, M., Fawkner-Corbett, D., Ashley, N., Cubitt, L., Mellado-Gomez, E., Attar, M., Sharma, E., Wills, Q., Bowden, R., Richter, F. C., Ahern, D., Puri, K. D., Henault, J., Gervais, F., Koohy, H. & Simmons, A. Structural Remodeling of the Human Colonic Mesenchyme in Inflammatory Bowel Disease. *Cell* **175**, 372-386 e317, doi:10.1016/j.cell.2018.08.067 (2018).

13 Harnack, C., Berger, H., Antanaviciute, A., Vidal, R., Sauer, S., Simmons, A., Meyer, T. F. & Sigal, M. R-spondin 3 promotes stem cell recovery and epithelial regeneration in the colon. *Nat Commun* **10**, 4368, doi:10.1038/s41467-019-12349-5 (2019).

14 McCarthy, N., Kraiczy, J. & Shivdasani, R. A. Cellular and molecular architecture of the intestinal stem cell niche. *Nat Cell Biol* **22**, 1033-1041, doi:10.1038/s41556-020-0567-z (2020).
15 Rafii, S., Butler, J. M. & Ding, B. S. Angiocrine functions of organ-specific endothelial cells. *Nature* **529**, 316-325, doi:10.1038/nature17040 (2016).
16 Drokhlyansky, E., Smillie, C. S., Van Wittenberghe, N., Ericsson, M., Griffin, G. K., Eraslan, G., Dionne, D., Cuoco, M. S., Goder-Reiser, M. N., Sharova, T., Kuksenko, O., Aguirre, A. J., Boland, G. M., Graham, D., Rozenblatt-Rosen, O., Xavier, R. J. & Regev, A. The Human and Mouse Enteric Nervous System at Single-Cell Resolution. *Cell* **182**, 1606-1622 e1623, doi:10.1016/j.cell.2020.08.003 (2020).
17 Biton, M., Haber, A. L., Rogel, N., Burgin, G., Beyaz, S., Schnell, A., Ashenberg, O., Su, C. W., Smillie, C., Shekhar, K., Chen, Z., Wu, C., Ordovas-Montanes, J., Alvarez, D., Herbst, R. H., Zhang, M., Tirosh, I., Dionne, D., Nguyen, L. T., Xifaras, M. E., Shalek, A. K., von Andrian, U. H., Graham, D. B., Rozenblatt-Rosen, O., Shi, H. N., Kuchroo, V., Yilmaz, O. H., Regev, A. & Xavier, R. J. T Helper Cell Cytokines Modulate Intestinal Stem Cell Renewal and Differentiation. *Cell* **175**, 1307-1320 e1322, doi:10.1016/j.cell.2018.10.008 (2018).
18 Rankin, L. C. & Artis, D. Beyond Host Defense: Emerging Functions of the Immune System in Regulating Complex Tissue Physiology. *Cell* **173**, 554-567, doi:10.1016/j.cell.2018.03.013 (2018).
19 Bar-Ephraim, Y. E., Kretzschmar, K. & Clevers, H. Organoids in immunological research. *Nat Rev Immunol* **20**, 279-293, doi:10.1038/s41577-019-0248-y (2020).
20 Hou, Q., Huang, J., Ayansola, H., Masatoshi, H. & Zhang, B. Intestinal Stem Cells and Immune Cell Relationships: Potential Therapeutic Targets for Inflammatory Bowel Diseases. *Front Immunol* **11**, 623691, doi:10.3389/fimmu.2020.623691 (2020).
21 Sehgal, A., Donaldson, D. S., Pridans, C., Sauter, K. A., Hume, D. A. & Mabbott, N. A. The role of CSF1R-dependent macrophages in control of the intestinal stem-cell niche. *Nat Commun* **9**, 1272, doi:10.1038/s41467-018-03638-6 (2018).
22 Saha, S., Aranda, E., Hayakawa, Y., Bhanja, P., Atay, S., Brodin, N. P., Li, J., Asfaha, S., Liu, L., Tailor, Y., Zhang, J., Godwin, A. K., Tome, W. A., Wang, T. C., Guha, C. & Pollard, J. W. Macrophage-derived extracellular vesicle-packaged WNTs rescue intestinal stem cells and enhance survival after radiation injury. *Nat Commun* **7**, 13096, doi:10.1038/ncomms13096 (2016).
23 Ogasawara, R., Hashimoto, D., Kimura, S., Hayase, E., Ara, T., Takahashi, S., Ohigashi, H., Yoshioka, K., Tateno, T., Yokoyama, E., Ebata, K., Kondo, T., Sugita, J., Onozawa, M., Iwanaga, T. & Teshima, T. Intestinal Lymphatic Endothelial Cells Produce R-Spondin3. *Sci Rep* **8**, 10719, doi:10.1038/s41598-018-29100-7 (2018).
24 Bergers, G. & Song, S. The role of pericytes in blood-vessel formation and maintenance. *Neuro Oncol* **7**, 452-464, doi:10.1215/S1152851705000232 (2005).
25 Armulik, A., Genove, G. & Betsholtz, C. Pericytes: developmental, physiological, and pathological perspectives, problems, and promises. *Dev Cell* **21**, 193-215, doi:10.1016/j.devcel.2011.07.001 (2011).
26 Gerhardt, H., Golding, M., Fruttiger, M., Ruhrberg, C., Lundkvist, A., Abramsson, A., Jeltsch, M., Mitchell, C., Alitalo, K., Shima, D. & Betsholtz, C. VEGF guides angiogenic sprouting utilizing endothelial tip cell filopodia. *J Cell Biol* **161**, 1163-1177, doi:10.1083/jcb.200302047 (2003).
27 Sundberg, C., Kowanetz, M., Brown, L. F., Detmar, M. & Dvorak, H. F. Stable expression of angiopoietin-1 and other markers by cultured pericytes: phenotypic

similarities to a subpopulation of cells in maturing vessels during later stages of angiogenesis in vivo. *Lab Invest* **82**, 387-401, doi:10.1038/labinvest.3780433 (2002).

28 Sigal, M., Logan, C. Y., Kapalczynska, M., Mollenkopf, H. J., Berger, H., Wiedenmann, B., Nusse, R., Amieva, M. R. & Meyer, T. F. Stromal R-spondin orchestrates gastric epithelial stem cells and gland homeostasis. *Nature* **548**, 451-455, doi:10.1038/nature23642 (2017).

29 McCarthy, N., Manieri, E., Storm, E. E., Saadatpour, A., Luoma, A. M., Kapoor, V. N., Madha, S., Gaynor, L. T., Cox, C., Keerthivasan, S., Wucherpfennig, K., Yuan, G. C., de Sauvage, F. J., Turley, S. J. & Shivdasani, R. A. Distinct Mesenchymal Cell Populations Generate the Essential Intestinal BMP Signaling Gradient. *Cell Stem Cell* **26**, 391-402 e395, doi:10.1016/j.stem.2020.01.008 (2020).

30 Stzepourginski, I., Nigro, G., Jacob, J. M., Dulauroy, S., Sansonetti, P. J., Eberl, G. & Peduto, L. CD34+ mesenchymal cells are a major component of the intestinal stem cells niche at homeostasis and after injury. *Proc Natl Acad Sci U S A* **114**, E506-E513, doi:10.1073/pnas.1620059114 (2017).

31 Wu, N., Sun, H., Zhao, X., Zhang, Y., Tan, J., Qi, Y., Wang, Q., Ng, M., Liu, Z., He, L., Niu, X., Chen, L., Liu, Z., Li, H. B., Zeng, Y. A., Roulis, M., Liu, D., Cheng, J., Zhou, B., Ng, L. G., Zou, D., Ye, Y., Flavell, R. A., Ginhoux, F. & Su, B. MAP3K2-regulated intestinal stromal cells define a distinct stem cell niche. *Nature* **592**, 606-610, doi:10.1038/s41586-021-03283-y (2021).

32 Roulis, M., Kaklamanos, A., Schernthanner, M., Bielecki, P., Zhao, J., Kaffe, E., Frommelt, L. S., Qu, R., Knapp, M. S., Henriques, A., Chalkidi, N., Koliaraki, V., Jiao, J., Brewer, J. R., Bacher, M., Blackburn, H. N., Zhao, X., Breyer, R. M., Aidinis, V., Jain, D., Su, B., Herschman, H. R., Kluger, Y., Kollias, G. & Flavell, R. A. Paracrine orchestration of intestinal tumorigenesis by a mesenchymal niche. *Nature* **580**, 524-529, doi:10.1038/s41586-020-2166-3 (2020).

33 Lancaster, M. A. & Knoblich, J. A. Organogenesis in a dish: modeling development and disease using organoid technologies. *Science* **345**, 1247125, doi:10.1126/science.1247125 (2014).

34 Clevers, H. Modeling Development and Disease with Organoids. *Cell* **165**, 1586-1597, doi:10.1016/j.cell.2016.05.082 (2016).

35 Sato, T., Vries, R. G., Snippert, H. J., van de Wetering, M., Barker, N., Stange, D. E., van Es, J. H., Abo, A., Kujala, P., Peters, P. J. & Clevers, H. Single Lgr5 stem cells build crypt-villus structures in vitro without a mesenchymal niche. *Nature* **459**, 262-265, doi:10.1038/nature07935 (2009).

36 Sato, T., Stange, D. E., Ferrante, M., Vries, R. G., Van Es, J. H., Van den Brink, S., Van Houdt, W. J., Pronk, A., Van Gorp, J., Siersema, P. D. & Clevers, H. Long-term expansion of epithelial organoids from human colon, adenoma, adenocarcinoma, and Barrett's epithelium. *Gastroenterology* **141**, 1762-1772, doi:10.1053/j.gastro.2011.07.050 (2011).

37 Yin, X., Farin, H. F., van Es, J. H., Clevers, H., Langer, R. & Karp, J. M. Niche-independent high-purity cultures of Lgr5+ intestinal stem cells and their progeny. *Nat Methods* **11**, 106-112, doi:10.1038/nmeth.2737 (2014).

38 Fujii, M., Matano, M., Toshimitsu, K., Takano, A., Mikami, Y., Nishikori, S., Sugimoto, S. & Sato, T. Human Intestinal Organoids Maintain Self-Renewal Capacity and Cellular Diversity in Niche-Inspired Culture Condition. *Cell Stem Cell* **23**, 787-793 e786, doi:10.1016/j.stem.2018.11.016 (2018).

39 Heuberger, J., Trimpert, J., Vladimirova, D., Goosmann, C., Lin, M., Schmuck, R., Mollenkopf, H. J., Brinkmann, V., Tacke, F., Osterrieder, N. & Sigal, M. Epithelial

response to IFN-gamma promotes SARS-CoV-2 infection. *EMBO Mol Med* **13**, e13191, doi:10.15252/emmm.202013191 (2021).

40 Tuveson, D. & Clevers, H. Cancer modeling meets human organoid technology. *Science* **364**, 952-955, doi:10.1126/science.aaw6985 (2019).

41 Sugimoto, S., Kobayashi, E., Fujii, M., Ohta, Y., Arai, K., Matano, M., Ishikawa, K., Miyamoto, K., Toshimitsu, K., Takahashi, S., Nanki, K., Hakamata, Y., Kanai, T. & Sato, T. An organoid-based organ-repurposing approach to treat short bowel syndrome. *Nature* **592**, 99-104, doi:10.1038/s41586-021-03247-2 (2021).

42 Cruz-Acuna, R. & Garcia, A. J. Engineered materials to model human intestinal development and cancer using organoids. *Exp Cell Res* **377**, 109-114, doi:10.1016/j.yexcr.2019.02.017 (2019).

43 Zhang, Y. & Que, J. BMP Signaling in Development, Stem Cells, and Diseases of the Gastrointestinal Tract. *Annu Rev Physiol* **82**, 251-273, doi:10.1146/annurev-physiol-021119-034500 (2020).

44 Yamaguchi, K., Shirakabe, K., Shibuya, H., Irie, K., Oishi, I., Ueno, N., Taniguchi, T., Nishida, E. & Matsumoto, K. Identification of a member of the MAPKKK family as a potential mediator of TGF-beta signal transduction. *Science* **270**, 2008-2011, doi:10.1126/science.270.5244.2008 (1995).

45 Yanagita, M. BMP antagonists: their roles in development and involvement in pathophysiology. *Cytokine Growth Factor Rev* **16**, 309-317, doi:10.1016/j.cytogfr.2005.02.007 (2005).

46 Hardwick, J. C., Van Den Brink, G. R., Bleuming, S. A., Ballester, I., Van Den Brande, J. M., Keller, J. J., Offerhaus, G. J., Van Deventer, S. J. & Peppelenbosch, M. P. Bone morphogenetic protein 2 is expressed by, and acts upon, mature epithelial cells in the colon. *Gastroenterology* **126**, 111-121, doi:10.1053/j.gastro.2003.10.067 (2004).

47 Allaire, J. M., Roy, S. A., Ouellet, C., Lemieux, E., Jones, C., Paquet, M., Boudreau, F. & Perreault, N. Bmp signaling in colonic mesenchyme regulates stromal microenvironment and protects from polyposis initiation. *Int J Cancer* **138**, 2700-2712, doi:10.1002/ijc.30001 (2016).

48 Qi, Z., Li, Y., Zhao, B., Xu, C., Liu, Y., Li, H., Zhang, B., Wang, X., Yang, X., Xie, W., Li, B., Han, J. J. & Chen, Y. G. BMP restricts stemness of intestinal Lgr5(+) stem cells by directly suppressing their signature genes. *Nat Commun* **8**, 13824, doi:10.1038/ncomms13824 (2017).

49 Gregorieff, A. & Clevers, H. Wnt signaling in the intestinal epithelium: from endoderm to cancer. *Genes Dev* **19**, 877-890, doi:10.1101/gad.1295405 (2005).

50 Hansson, M., Olesen, D. R., Peterslund, J. M., Engberg, N., Kahn, M., Winzi, M., Klein, T., Maddox-Hyttel, P. & Serup, P. A late requirement for Wnt and FGF signaling during activin-induced formation of foregut endoderm from mouse embryonic stem cells. *Dev Biol* **330**, 286-304, doi:10.1016/j.ydbio.2009.03.026 (2009).

51 Madison, B. B., Braunstein, K., Kuizon, E., Portman, K., Qiao, X. T. & Gumucio, D. L. Epithelial hedgehog signals pattern the intestinal crypt-villus axis. *Development* **132**, 279-289, doi:10.1242/dev.01576 (2005).

52 van Es, J. H., van Gijn, M. E., Riccio, O., van den Born, M., Vooijs, M., Begthel, H., Cozijnsen, M., Robine, S., Winton, D. J., Radtke, F. & Clevers, H. Notch/gamma-secretase inhibition turns proliferative cells in intestinal crypts and adenomas into goblet cells. *Nature* **435**, 959-963, doi:10.1038/nature03659 (2005).

53 Roberts, D. J. Molecular mechanisms of development of the gastrointestinal tract. *Dev Dyn* **219**, 109-120, doi:10.1002/1097-0177(2000)9999:9999<::aid-dvdy1047>3.3.co;2-y (2000).
54 Zorn, A. M. & Wells, J. M. Vertebrate endoderm development and organ formation. *Annu Rev Cell Dev Biol* **25**, 221-251, doi:10.1146/annurev.cellbio.042308.113344 (2009).
55 Roberts, D. J., Smith, D. M., Goff, D. J. & Tabin, C. J. Epithelial-mesenchymal signaling during the regionalization of the chick gut. *Development* **125**, 2791-2801, doi:10.1242/dev.125.15.2791 (1998).
56 Wang, S. & Chen, Y. G. BMP signaling in homeostasis, transformation and inflammatory response of intestinal epithelium. *Sci China Life Sci* **61**, 800-807, doi:10.1007/s11427-018-9310-7 (2018).
57 Auclair, B. A., Benoit, Y. D., Rivard, N., Mishina, Y. & Perreault, N. Bone morphogenetic protein signaling is essential for terminal differentiation of the intestinal secretory cell lineage. *Gastroenterology* **133**, 887-896, doi:10.1053/j.gastro.2007.06.066 (2007).
58 Haramis, A. P., Begthel, H., van den Born, M., van Es, J., Jonkheer, S., Offerhaus, G. J. & Clevers, H. De novo crypt formation and juvenile polyposis on BMP inhibition in mouse intestine. *Science* **303**, 1684-1686, doi:10.1126/science.1093587 (2004).
59 Davis, H., Irshad, S., Bansal, M., Rafferty, H., Boitsova, T., Bardella, C., Jaeger, E., Lewis, A., Freeman-Mills, L., Giner, F. C., Rodenas-Cuadrado, P., Mallappa, S., Clark, S., Thomas, H., Jeffery, R., Poulsom, R., Rodriguez-Justo, M., Novelli, M., Chetty, R., Silver, A., Sansom, O. J., Greten, F. R., Wang, L. M., East, J. E., Tomlinson, I. & Leedham, S. J. Aberrant epithelial GREM1 expression initiates colonic tumorigenesis from cells outside the stem cell niche. *Nat Med* **21**, 62-70, doi:10.1038/nm.3750 (2015).
60 Means, A. L., Freeman, T. J., Zhu, J., Woodbury, L. G., Marincola-Smith, P., Wu, C., Meyer, A. R., Weaver, C. J., Padmanabhan, C., An, H., Zi, J., Wessinger, B. C., Chaturvedi, R., Brown, T. D., Deane, N. G., Coffey, R. J., Wilson, K. T., Smith, J. J., Sawyers, C. L., Goldenring, J. R., Novitskiy, S. V., Washington, M. K., Shi, C. & Beauchamp, R. D. Epithelial Smad4 Deletion Up-Regulates Inflammation and Promotes Inflammation-Associated Cancer. *Cell Mol Gastroenterol Hepatol* **6**, 257-276, doi:10.1016/j.jcmgh.2018.05.006 (2018).
61 Voorneveld, P. W., Kodach, L. L., Jacobs, R. J., Liv, N., Zonnevylle, A. C., Hoogenboom, J. P., Biemond, I., Verspaget, H. W., Hommes, D. W., de Rooij, K., van Noesel, C. J., Morreau, H., van Wezel, T., Offerhaus, G. J., van den Brink, G. R., Peppelenbosch, M. P., Ten Dijke, P. & Hardwick, J. C. Loss of SMAD4 alters BMP signaling to promote colorectal cancer cell metastasis via activation of Rho and ROCK. *Gastroenterology* **147**, 196-208 e113, doi:10.1053/j.gastro.2014.03.052 (2014).
62 Voorneveld, P. W., Kodach, L. L., Jacobs, R. J., van Noesel, C. J., Peppelenbosch, M. P., Korkmaz, K. S., Molendijk, I., Dekker, E., Morreau, H., van Pelt, G. W., Tollenaar, R. A., Mesker, W., Hawinkels, L. J., Paauwe, M., Verspaget, H. W., Geraets, D. T., Hommes, D. W., Offerhaus, G. J., van den Brink, G. R., Ten Dijke, P. & Hardwick, J. C. The BMP pathway either enhances or inhibits the Wnt pathway depending on the SMAD4 and p53 status in CRC. *Br J Cancer* **112**, 122-130, doi:10.1038/bjc.2014.560 (2015).

63 van Amerongen, R., Bowman, A. N. & Nusse, R. Developmental stage and time dictate the fate of Wnt/beta-catenin-responsive stem cells in the mammary gland. *Cell Stem Cell* **11**, 387-400, doi:10.1016/j.stem.2012.05.023 (2012).

64 Madisen, L., Zwingman, T. A., Sunkin, S. M., Oh, S. W., Zariwala, H. A., Gu, H., Ng, L. L., Palmiter, R. D., Hawrylycz, M. J., Jones, A. R., Lein, E. S. & Zeng, H. A robust and high-throughput Cre reporting and characterization system for the whole mouse brain. *Nat Neurosci* **13**, 133-140, doi:10.1038/nn.2467 (2010).

65 Mishina, Y., Hanks, M. C., Miura, S., Tallquist, M. D. & Behringer, R. R. Generation of Bmpr/Alk3 conditional knockout mice. *Genesis* **32**, 69-72, doi:10.1002/gene.10038 (2002).

66 Hadjantonakis, A. K., Macmaster, S. & Nagy, A. Embryonic stem cells and mice expressing different GFP variants for multiple non-invasive reporter usage within a single animal. *BMC Biotechnol* **2**, 11, doi:10.1186/1472-6750-2-11 (2002).

67 Vintersten, K., Monetti, C., Gertsenstein, M., Zhang, P., Laszlo, L., Biechele, S. & Nagy, A. Mouse in red: red fluorescent protein expression in mouse ES cells, embryos, and adult animals. *Genesis* **40**, 241-246, doi:10.1002/gene.20095 (2004).

68 Satija, R., Farrell, J. A., Gennert, D., Schier, A. F. & Regev, A. Spatial reconstruction of single-cell gene expression data. *Nat Biotechnol* **33**, 495-502, doi:10.1038/nbt.3192 (2015).

69 Jin, S., Guerrero-Juarez, C. F., Zhang, L., Chang, I., Ramos, R., Kuan, C. H., Myung, P., Plikus, M. V. & Nie, Q. Inference and analysis of cell-cell communication using CellChat. *Nat Commun* **12**, 1088, doi:10.1038/s41467-021-21246-9 (2021).

70 Lustig, B., Jerchow, B., Sachs, M., Weiler, S., Pietsch, T., Karsten, U., van de Wetering, M., Clevers, H., Schlag, P. M., Birchmeier, W. & Behrens, J. Negative feedback loop of Wnt signaling through upregulation of conductin/axin2 in colorectal and liver tumors. *Mol Cell Biol* **22**, 1184-1193, doi:10.1128/MCB.22.4.1184-1193.2002 (2002).

71 Cai, J., Zhang, N., Zheng, Y., de Wilde, R. F., Maitra, A. & Pan, D. The Hippo signaling pathway restricts the oncogenic potential of an intestinal regeneration program. *Genes Dev* **24**, 2383-2388, doi:10.1101/gad.1978810 (2010).

72 Yui, S., Azzolin, L., Maimets, M., Pedersen, M. T., Fordham, R. P., Hansen, S. L., Larsen, H. L., Guiu, J., Alves, M. R. P., Rundsten, C. F., Johansen, J. V., Li, Y., Madsen, C. D., Nakamura, T., Watanabe, M., Nielsen, O. H., Schweiger, P. J., Piccolo, S. & Jensen, K. B. YAP/TAZ-Dependent Reprogramming of Colonic Epithelium Links ECM Remodeling to Tissue Regeneration. *Cell Stem Cell* **22**, 35-49 e37, doi:10.1016/j.stem.2017.11.001 (2018).

73 Moya, I. M. & Halder, G. Hippo-YAP/TAZ signalling in organ regeneration and regenerative medicine. *Nat Rev Mol Cell Biol* **20**, 211-226, doi:10.1038/s41580-018-0086-y (2019).

74 Ricard-Blum, S. The collagen family. *Cold Spring Harb Perspect Biol* **3**, a004978, doi:10.1101/cshperspect.a004978 (2011).

75 Domogatskaya, A., Rodin, S. & Tryggvason, K. Functional diversity of laminins. *Annu Rev Cell Dev Biol* **28**, 523-553, doi:10.1146/annurev-cellbio-101011-155750 (2012).

76 Shoshkes-Carmel, M., Wang, Y. J., Wangensteen, K. J., Toth, B., Kondo, A., Massasa, E. E., Itzkovitz, S. & Kaestner, K. H. Subepithelial telocytes are an important source of Wnts that supports intestinal crypts. *Nature* **557**, 242-246, doi:10.1038/s41586-018-0084-4 (2018).

77 Greicius, G., Kabiri, Z., Sigmundsson, K., Liang, C., Bunte, R., Singh, M. K. & Virshup, D. M. PDGFRalpha(+) pericryptal stromal cells are the critical source of Wnts and RSPO3 for murine intestinal stem cells in vivo. *Proc Natl Acad Sci U S A* **115**, E3173-E3181, doi:10.1073/pnas.1713510115 (2018).

78 Miyoshi, H., Ajima, R., Luo, C. T., Yamaguchi, T. P. & Stappenbeck, T. S. Wnt5a potentiates TGF-beta signaling to promote colonic crypt regeneration after tissue injury. *Science* **338**, 108-113, doi:10.1126/science.1223821 (2012).

79 Bao, S., Ouyang, G., Bai, X., Huang, Z., Ma, C., Liu, M., Shao, R., Anderson, R. M., Rich, J. N. & Wang, X. F. Periostin potently promotes metastatic growth of colon cancer by augmenting cell survival via the Akt/PKB pathway. *Cancer Cell* **5**, 329-339, doi:10.1016/s1535-6108(04)00081-9 (2004).

80 Kapalczynska, M., Lin, M., Maertzdorf, J., Heuberger, J., Muellerke, S., Zuo, X., Vidal, R., Shureiqi, I., Fischer, A. S., Sauer, S., Berger, H., Kidess, E., Mollenkopf, H. J., Tacke, F., Meyer, T. F. & Sigal, M. BMP feed-forward loop promotes terminal differentiation in gastric glands and is interrupted by H. pylori-driven inflammation. *Nat Commun* **13**, 1577, doi:10.1038/s41467-022-29176-w (2022).

81 Kosinski, C., Li, V. S., Chan, A. S., Zhang, J., Ho, C., Tsui, W. Y., Chan, T. L., Mifflin, R. C., Powell, D. W., Yuen, S. T., Leung, S. Y. & Chen, X. Gene expression patterns of human colon tops and basal crypts and BMP antagonists as intestinal stem cell niche factors. *Proc Natl Acad Sci U S A* **104**, 15418-15423, doi:10.1073/pnas.0707210104 (2007).

82 De Robertis, M., Massi, E., Poeta, M. L., Carotti, S., Morini, S., Cecchetelli, L., Signori, E. & Fazio, V. M. The AOM/DSS murine model for the study of colon carcinogenesis: From pathways to diagnosis and therapy studies. *J Carcinog* **10**, 9, doi:10.4103/1477-3163.78279 (2011).

83 Gregorieff, A., Liu, Y., Inanlou, M. R., Khomchuk, Y. & Wrana, J. L. Yap-dependent reprogramming of Lgr5(+) stem cells drives intestinal regeneration and cancer. *Nature* **526**, 715-718, doi:10.1038/nature15382 (2015).

84 Rossi, G., Manfrin, A. & Lutolf, M. P. Progress and potential in organoid research. *Nat Rev Genet* **19**, 671-687, doi:10.1038/s41576-018-0051-9 (2018).

85 Qin, X., Sufi, J., Vlckova, P., Kyriakidou, P., Acton, S. E., Li, V. S. W., Nitz, M. & Tape, C. J. Cell-type-specific signaling networks in heterocellular organoids. *Nat Methods* **17**, 335-342, doi:10.1038/s41592-020-0737-8 (2020).

86 Boccellato, F., Woelffling, S., Imai-Matsushima, A., Sanchez, G., Goosmann, C., Schmid, M., Berger, H., Morey, P., Denecke, C., Ordemann, J. & Meyer, T. F. Polarised epithelial monolayers of the gastric mucosa reveal insights into mucosal homeostasis and defence against infection. *Gut* **68**, 400-413, doi:10.1136/gutjnl-2017-314540 (2019).

87 Palikuqi, B., Nguyen, D. T., Li, G., Schreiner, R., Pellegata, A. F., Liu, Y., Redmond, D., Geng, F., Lin, Y., Gomez-Salinero, J. M., Yokoyama, M., Zumbo, P., Zhang, T., Kunar, B., Witherspoon, M., Han, T., Tedeschi, A. M., Scottoni, F., Lipkin, S. M., Dow, L., Elemento, O., Xiang, J. Z., Shido, K., Spence, J. R., Zhou, Q. J., Schwartz, R. E., De Coppi, P., Rabbany, S. Y. & Rafii, S. Adaptable haemodynamic endothelial cells for organogenesis and tumorigenesis. *Nature* **585**, 426-432, doi:10.1038/s41586-020-2712-z (2020).

88 Matsuzawa-Ishimoto, Y., Hine, A., Shono, Y., Rudensky, E., Lazrak, A., Yeung, F., Neil, J. A., Yao, X., Chen, Y. H., Heaney, T., Schuster, S. L., Zwack, E. E., Axelrad, J. E., Hudesman, D., Tsai, J. J., Nichols, K., Dewan, M. Z., Cammer, M., Beal, A., Hoffman, S., Geddes, B., Bertin, J., Liu, C., Torres, V. J., Loke, P., van den Brink, M. R. M. & Cadwell, K. An intestinal organoid-based platform that recreates

susceptibility to T-cell-mediated tissue injury. *Blood* **135**, 2388-2401, doi:10.1182/blood.2019004116 (2020).

89 Eicher, A. K., Kechele, D. O., Sundaram, N., Berns, H. M., Poling, H. M., Haines, L. E., Sanchez, J. G., Kishimoto, K., Krishnamurthy, M., Han, L., Zorn, A. M., Helmrath, M. A. & Wells, J. M. Functional human gastrointestinal organoids can be engineered from three primary germ layers derived separately from pluripotent stem cells. *Cell Stem Cell* **29**, 36-51 e36, doi:10.1016/j.stem.2021.10.010 (2022).

90 Workman, M. J., Mahe, M. M., Trisno, S., Poling, H. M., Watson, C. L., Sundaram, N., Chang, C. F., Schiesser, J., Aubert, P., Stanley, E. G., Elefanty, A. G., Miyaoka, Y., Mandegar, M. A., Conklin, B. R., Neunlist, M., Brugmann, S. A., Helmrath, M. A. & Wells, J. M. Engineered human pluripotent-stem-cell-derived intestinal tissues with a functional enteric nervous system. *Nat Med* **23**, 49-59, doi:10.1038/nm.4233 (2017).

91 Kim, E., Choi, S., Kang, B., Kong, J., Kim, Y., Yoon, W. H., Lee, H. R., Kim, S., Kim, H. M., Lee, H., Yang, C., Lee, Y. J., Kang, M., Roh, T. Y., Jung, S., Kim, S., Ku, J. H. & Shin, K. Creation of bladder assembloids mimicking tissue regeneration and cancer. *Nature* **588**, 664-669, doi:10.1038/s41586-020-3034-x (2020).

92 Koppens, M. A. J., Davis, H., Valbuena, G. N., Mulholland, E. J., Nasreddin, N., Colombe, M., Antanaviciute, A., Biswas, S., Friedrich, M., Lee, L., Oxford, I. B. D. C. I., Wang, L. M., Koelzer, V. H., East, J. E., Simmons, A., Winton, D. J. & Leedham, S. J. Bone Morphogenetic Protein Pathway Antagonism by Grem1 Regulates Epithelial Cell Fate in Intestinal Regeneration. *Gastroenterology* **161**, 239-254 e239, doi:10.1053/j.gastro.2021.03.052 (2021).

93 Degirmenci, B., Valenta, T., Dimitrieva, S., Hausmann, G. & Basler, K. GLI1-expressing mesenchymal cells form the essential Wnt-secreting niche for colon stem cells. *Nature* **558**, 449-453, doi:10.1038/s41586-018-0190-3 (2018).

94 Beumer, J., Puschhof, J., Yengej, F. Y., Zhao, L., Martinez-Silgado, A., Blotenburg, M., Begthel, H., Boot, C., van Oudenaarden, A., Chen, Y. G. & Clevers, H. BMP gradient along the intestinal villus axis controls zonated enterocyte and goblet cell states. *Cell Rep* **38**, 110438, doi:10.1016/j.celrep.2022.110438 (2022).

95 Maloum, F., Allaire, J. M., Gagne-Sansfacon, J., Roy, E., Belleville, K., Sarret, P., Morisset, J., Carrier, J. C., Mishina, Y., Kaestner, K. H. & Perreault, N. Epithelial BMP signaling is required for proper specification of epithelial cell lineages and gastric endocrine cells. *Am J Physiol Gastrointest Liver Physiol* **300**, G1065-1079, doi:10.1152/ajpgi.00176.2010 (2011).

96 Shinohara, M., Mao, M., Keeley, T. M., El-Zaatari, M., Lee, H. J., Eaton, K. A., Samuelson, L. C., Merchant, J. L., Goldenring, J. R. & Todisco, A. Bone morphogenetic protein signaling regulates gastric epithelial cell development and proliferation in mice. *Gastroenterology* **139**, 2050-2060 e2052, doi:10.1053/j.gastro.2010.08.052 (2010).

97 Kaestner, K. H., Silberg, D. G., Traber, P. G. & Schutz, G. The mesenchymal winged helix transcription factor Fkh6 is required for the control of gastrointestinal proliferation and differentiation. *Genes Dev* **11**, 1583-1595, doi:10.1101/gad.11.12.1583 (1997).

98 Walton, K. D., Kolterud, A., Czerwinski, M. J., Bell, M. J., Prakash, A., Kushwaha, J., Grosse, A. S., Schnell, S. & Gumucio, D. L. Hedgehog-responsive mesenchymal clusters direct patterning and emergence of intestinal villi. *Proc Natl Acad Sci U S A* **109**, 15817-15822, doi:10.1073/pnas.1205669109 (2012).

99 Rao-Bhatia, A., Zhu, M., Yin, W. C., Coquenlorge, S., Zhang, X., Woo, J., Sun, Y., Dean, C. H., Liu, A., Hui, C. C., Shivdasani, R. A., McNeill, H., Hopyan, S. & Kim,

T. H. Hedgehog-Activated Fat4 and PCP Pathways Mediate Mesenchymal Cell Clustering and Villus Formation in Gut Development. *Dev Cell* **52**, 647-658 e646, doi:10.1016/j.devcel.2020.02.003 (2020).

100 Junttila, M. R. & de Sauvage, F. J. Influence of tumour micro-environment heterogeneity on therapeutic response. *Nature* **501**, 346-354, doi:10.1038/nature12626 (2013).

101 Polanska, U. M. & Orimo, A. Carcinoma-associated fibroblasts: non-neoplastic tumour-promoting mesenchymal cells. *J Cell Physiol* **228**, 1651-1657, doi:10.1002/jcp.24347 (2013).

102 Yamashita, M., Ogawa, T., Zhang, X., Hanamura, N., Kashikura, Y., Takamura, M., Yoneda, M. & Shiraishi, T. Role of stromal myofibroblasts in invasive breast cancer: stromal expression of alpha-smooth muscle actin correlates with worse clinical outcome. *Breast Cancer* **19**, 170-176, doi:10.1007/s12282-010-0234-5 (2012).

103 Fujita, H., Ohuchida, K., Mizumoto, K., Nakata, K., Yu, J., Kayashima, T., Cui, L., Manabe, T., Ohtsuka, T. & Tanaka, M. alpha-Smooth Muscle Actin Expressing Stroma Promotes an Aggressive Tumor Biology in Pancreatic Ductal Adenocarcinoma. *Pancreas* **39**, 1254-1262, doi:10.1097/MPA.0b013e3181dbf647 (2010).

104 Cromer, W. E., Mathis, J. M., Granger, D. N., Chaitanya, G. V. & Alexander, J. S. Role of the endothelium in inflammatory bowel diseases. *World J Gastroenterol* **17**, 578-593, doi:10.3748/wjg.v17.i5.578 (2011).

Statutory declaration

“I, Manqiang Lin, by personally signing this document in lieu of an oath, hereby affirm that I prepared the submitted dissertation on the topic Generation of colon assembloids modeling epithelial-stromal interaction and self-organization (Erzeugung von Kolon-Assembloiden zur Modellierung der Epithel-Stroma Interaktion und Selbstor-ganisation), independently and without the support of third parties, and that I used no other sources and aids than those stated.

All parts which are based on the publications or presentations of other authors, either in letter or in spirit, are specified as such in accordance with the citing guidelines. The sections on methodology (in particular regarding practical work, laboratory regulations, statistical processing) and results (in particular regarding figures, charts and tables) are exclusively my responsibility.

Furthermore, I declare that I have correctly marked all of the data, the analyses, and the conclusions generated from data obtained in collaboration with other persons, and that I have correctly marked my own contribution and the contributions of other persons (cf. declaration of contribution). I have correctly marked all texts or parts of texts that were generated in collaboration with other persons.

My contributions to any publications to this dissertation correspond to those stated in the below joint declaration made together with the supervisor. All publications created within the scope of the dissertation comply with the guidelines of the ICMJE (International Committee of Medical Journal Editors; www.icmje.org) on authorship. In addition, I declare that I shall comply with the regulations of Charité – Universitätsmedizin Berlin on ensuring good scientific practice.

I declare that I have not yet submitted this dissertation in identical or similar form to another Faculty.

The significance of this statutory declaration and the consequences of a false statutory declaration under criminal law (Sections 156, 161 of the German Criminal Code) are known to me.”

Date	Signature

Curriculum vitae

My curriculum vitae does not appear in the electronic version of my paper for reasons of data protection.

Complete list of publications

1. **Lin M**, Hartl K, Heuberger J, Li H, Berger H, Liu L, Heymann F, Woehler A, Tacke F, Rajewsky N, Sigal M. Assembloids reveal a crucial interplay between epithelium and stroma during gastrointestinal crypt maturation. Nat Commun. (In revision).
2. Kapalczynska M*, **Lin M***, Maertzdorf J, Heuberger J, Muellerke S, Zuo X, Vidal R, Shureiqi I, Fischer AS, Sauer S, Berger H, Kidess E, Mollenkopf HJ, Tacke F, Meyer TF, Sigal M. BMP feed-forward loop promotes terminal differentiation in gastric glands and is interrupted by H. pylori-driven inflammation. Nat Commun. 2022 Mar 24;13(1):1577. doi: 10.1038/s41467-022-29176-w.
3. Wizenty J, Müllerke S, Kolesnichenko M, Heuberger J, **Lin M**, Fischer AS, Mollenkopf HJ, Berger H, Tacke F, Sigal M. Gastric stem cells promote inflammation and gland remodeling in response to Helicobacter pylori via Rspo3-Lgr4 axis. EMBO J. 2022 Jul 4;41(13):e109996. doi: 10.15252/embj.2021109996.
4. Fischer AS, Müllerke S, Arnold A, Heuberger J, Berger H, **Lin M**, Mollenkopf HJ, Wizenty J, Horst D, Tacke F, Sigal M. R-spondin/YAP axis promotes gastric oxyntic gland regeneration and Helicobacter pylori-associated metaplasia in mice. J Clin Invest. 2022 Nov 1;132(21):e151363. doi: 10.1172/JCI151363.
5. Heuberger J, Trimpert J, Vladimirova D, Goosmann C, **Lin M**, Schmuck R, Mollenkopf HJ, Brinkmann V, Tacke F, Osterrieder N, Sigal M. Epithelial response to IFN-γ promotes SARS-CoV-2 infection. EMBO Mol Med. 2021 Apr 9;13(4):e13191. doi: 10.15252/emmm.202013191.
6. Wang J*, **Lin M***, Xie J, Lin J, Lu J, Chen Q, Cao L, Lin M, Tu R, Li P, Zheng C, Huang C. BMI-adjusted prognosis of signet ring cell carcinoma in patients undergoing radical gastrectomy for gastric adenocarcinoma. Asian J Surg. 2021 Jan;44(1):116-122. doi: 10.1016/j.asjsur.2020.03.023.
7. **Lin M***, Wang J*, Zheng C, Li P, Xie J, Lin J, Lu J, Chen Q, Cao L, Lin M, He Q, Huang C. A modified subclassification to evaluate the survival of patients with N3 gastric cancer: an international database study. BMC Cancer. 2019 Jan 7;19(1):21. doi: 10.1186/s12885-018-5187-7.
8. Zheng C*, Wang J*, **Lin M**, Zhang P, Liu L, Lin J, Lu J, Chen Q, Cao L, Lin M, Tu R, Xie J, Li P, Huang C. CDK5RAP3 suppresses Wnt/β-catenin signaling by inhibiting AKT phosphorylation in gastric cancer. J Exp Clin Cancer Res. 2018 Mar 14;37(1):59. doi: 10.1186/s13046-018-0716-4.

9. Wang J*, **Lin M***, Li P, Xie J, Lin J, Lu J, Chen Q, Cao L, Lin M, Zheng C, Huang C. The prognostic relevance of parapyloric lymph node metastasis in Siewert type II/III adenocarcinoma of the esophagogastric junction. Eur J Surg Oncol. 2017 Dec;43(12):2333-2340. doi: 10.1016/j.ejso.2017.08.017.
10. Chen F, Zhuang M, Peng J, Wang X, Huang T, Li S, **Lin M**, Lin H, Xu Y, Li J, Chen Z, Huang Y. Baicalein inhibits migration and invasion of gastric cancer cells through suppression of the TGF-β signaling pathway. Mol Med Rep. 2014 Oct;10(4):1999-2003. doi: 10.3892/mmr.2014.2452.

Co-first author.

Acknowledgments

I turned 29 this year and have become more sensitive to time than ever before. More than a thousand days and nights have passed since the plane landed at Tegel Airport in Berlin on a brisk autumn evening in September 2018, to writing my thesis at the desk on a spring afternoon today in March 2022. It is already time to give thanks and prepare for my farewell.

First of all, I would like to thank my supervisor, Prof. Dr. Michael Sigal, for providing me with the precious opportunity to be part of his group. Every conversation I had with him during my doctoral study always give me different inspiration. He taught me how to find questions and how to keep digging when observing interesting phenomena, which is of great benefit to my academic career. He taught me how to face failure and to find something valuable in it. Whenever I showed him terrible experimental results, he always seemed calm and "blindly" optimistic. That gave me the courage to try again and to persevere. In addition, he gave me enough freedom to explore what I was interested in, which made me like science more and more. I would also like to thank Prof. Thomas Meyer, Prof. Dr. Bertram Wiedenmann, and Prof. Dr. Frank Tacke for providing me with a great research platform and support to complete my doctoral study. I am really grateful to the China Scholarship Council for providing me with a four-year scholarship to study in Germany. Many thanks to Franziska Grimm at Charite Welcome Center for helping me a lot when I first came to Charite.

I would like to thank my former and current lab colleagues and my friends. Special thanks to Stefanie Müllerke and Janine Wolff for keeping our lab organized and helping me a lot with animal experiments. Thank you to Christine Harnack for teaching me many experimental techniques when I first joined the lab, as well as being warm-hearted and making me feel at home in the lab. Thank you to Marta Kapalczynska, it was a pleasure to work with her on a project, she always had a big smile on her face and kindly shared me her knowledge. Thanks to Kimberly Hartl (first of all I would like to apologize for accidentally knocking her down while sledding in Ringberg in 2019), she is always eager to help others and keeps the sun shining in our lab, also we had a great collaboration on the assembloid project. Thanks to Anne-Sophie Fischer, we shared experience and discussed with each other when experiments got problems, and hope you will finish up your doctoral study

soon. Thanks to Julian Heuberger, who is always eager to give valuable suggestions. I am very grateful to the other members of our group, Jonas Wizenty (for helping me with the German translation of the abstract), Lichao Liu (for helping me with some experiments), Giulia Beccaceci, and Felix Bolduan, with whom I was very lucky to work. I would like to thank my other colleagues who helped me, Rike Zietlow for revising my manuscripts, who taught me a lot of writing skills; Hao Li and Hilmar Berger for helping me analyze the scRNA-seq data; Felix Heymann for providing me with mouse lines; Linda Hammerich and Ines Eichhorn for their organization for the lab. Thank you to my former Chinese partners at Max Planck Institute, Simeng Liu, Qilan Hong, Junxue Dong, Xianhe Li, and Xinming Yang, I always miss the time with you. Thanks to Xuewen Hou and Yang Yang, we came from China to Germany for our doctoral studies, helped each other along the way, and went on trips together. Thank you Junquan Pan, we met on the plane to Germany, and he showed me around when I first came to Berlin. Thanks to Shangxuan Gao, Eming Li, we met in Berlin when I looked for a flat, and I always miss our time as roommates, playing mobile games and traveling around Germany.

Lastly, I would like to thank my family. Thank you to my parents for always being selfless and giving of themselves to their children, and for always encouraging me to pursue my studies. Thank you to my sister and my brother for taking care of our family. I would like to thank my girlfriend Qiuhua Li. We have been together for almost ten years. We have experienced what each other has experienced and felt what each other has felt. We have been through the same seasons, and we have traveled to the same places. We are the only persons who know the hardships of our journey, and we also remember the joys forever. You comfort me when I am down, and share the happiness with me when I am successful. Because of you, I have made it this far. Thank you for your constant companionship and support.

Confirmation by a statistician

CHARITÉ

CharitéCentrum für Human- und Gesundheitswissenschaften

Charité | Campus Charité Mitte | 10117 Berlin

Institut für Biometrie und klinische Epidemiologie (iBikE)

Direktor: Prof. Dr. Frank Konietschke

Postantschrift:
Charitéplatz 1 | 10117 Berlin
Besucheranschrift:
Reinhardtstr. 58 | 10117 Berlin

Tel. +49 (0)30 450 562 161
frank.konietschke@charite.de
https://biometrie.charite.de/

Name, Vorname: Lin, Manqiang

Emailadresse: manqiang.lin@charite.de

Matrikelnummer: 226570

PromotionsbetreuerIn: Prof. Dr. Michael Sigal

Promotionsinstitution / Klinik: Medizinische Klinik mit Schwerpunkt Hepatologie und Gastroenterologie

Bescheinigung

Hiermit bescheinige ich, dass Herr Lin innerhalb der Service Unit Biometrie des Instituts für Biometrie und klinische Epidemiologie (iBikE) bei mir eine statistische Beratung zu einem Promotionsvorhaben wahrgenommen hat. Folgende Beratungstermine wurden wahrgenommen:

- Termin 1: 06.04.22

Folgende wesentliche Ratschläge hinsichtlich einer sinnvollen Auswertung und Interpretation der Daten wurden während der Beratung erteilt:

- Anstelle von parametrischen Tests sollten nicht-parametrische Tests genutzt werden, aufgrund der kleinen Fallzahlen (Kruskall Wallis anstelle von ANOVA, Wilcoxon oder Mann-Whitney Test anstelle vom t-Test für verbundene oder unverbundene Stichproben)
- Der Fokus sollte auf einer deskriptiven Auswertung liegen.

Diese Bescheinigung garantiert nicht die richtige Umsetzung der in der Beratung gemachten Vorschläge, die korrekte Durchführung der empfohlenen statistischen Verfahren und die richtige Darstellung und Interpretation der Ergebnisse. Die Verantwortung hierfür obliegt allein dem Promovierenden. Das Institut für Biometrie und klinische Epidemiologie übernimmt hierfür keine Haftung.

Datum: 04.05.2022 Name der Beraterin: Nilufar Akbari

Nilufar Akbari

Digital unterschrieben von Nilufar Akbari
Datum: 2022.05.04 15:13:07 +02'00'

CHARITÉ UNIVERSITÄTSMEDIZIN BERLIN Institut für Biometrie und Klinische Epidemiologie Campus Charité Mitte Charitéplatz 1 | D-10117 Berlin Reinhardtstr. 58

Unterschrift BeraterIn, Institutsstempel